

---

# SPECTRAL MIXTURE KERNELS WITH TIME AND PHASE DELAY DEPENDENCIES FOR GAUSSIAN PROCESSES

---

A PREPRINT

**Kai Chen**

Shenzhen Institutes of Advanced Technology, Chinese Academy of Sciences  
Shenzhen College of Advanced Technology, University of Chinese Academy of Sciences  
Institute for Computing and Information Sciences, Radboud University  
kchen@cs.ru.nl

**Twan van Laarhoven**

Institute for Computing and Information Sciences, Radboud University  
Faculty of Management, Science and Technology, Open University of The Netherlands  
twanvl@gmail.com

**Jinsong Chen**

Shenzhen Institutes of Advanced Technology, Chinese Academy of Sciences  
js.chen@siat.ac.cn

**Elena Marchiori**

Institute for Computing and Information Sciences, Radboud University  
elenam@cs.ru.nl

November 10, 2021

## ABSTRACT

Spectral Mixture (SM) kernels form a powerful class of kernels for Gaussian processes, capable to discover patterns, extrapolate, and model negative covariances. Being a linear superposition of quasi-periodical Gaussian components, an SM kernel does not explicitly model dependencies between components. In this paper we investigate the benefits of modeling explicitly time and phase delay dependencies between components in an AM kernel. We analyze the presence of statistical dependencies between components using Gaussian conditionals and posterior covariance and use this framework to motivate the proposed SM kernel extension, called Spectral Mixture kernel with time and phase delay Dependencies (SMD). SMD is constructed in two steps: first, time delay and phase delay are incorporated into each base component; next, cross-convolution between a base component and the reversed complex conjugate of another base component is performed which yields a complex-valued and positive definite kernel representing correlations between base components. The number of hyper-parameters of SMD, except the time and phase delay ones, remains equal to that of the SM kernel. We perform a thorough comparative experimental analysis of SMD on synthetic and real-life data sets. Results indicate the beneficial effect of modeling time and phase delay dependencies between base components, notably for natural phenomena involving little or no influence from human activity.

## 1 Introduction

Gaussian Processes (GPs) are an elegant Bayesian approach to model an unknown function. They provide regression models where a posterior distribution over the unknown function is maintained as evidence is accumulated. This allows

Gaussian processes to learn involved functions if a large amount of evidence is available and makes them robust against overfitting in the presence of little evidence [1, 2]. A GP can model a large class of phenomena through the choice of its kernel, which characterizes one’s assumption on how the unknown function autocovaries. The choice of kernel is a core aspect of the GP design, since the posterior distribution can significantly vary for different kernels.

Recently, [3] introduced a flexible kernel called Spectral Mixture (SM) by modeling its power spectral density with a sum of Gaussians. SM kernels can be represented by a sum of  $Q$  components which can be derived from Bochner’s theorem as the inverse Fourier transform of their corresponding spectral density functions. SM kernels for GPs have been shown to be effective for discovering latent patterns in datasets and for extrapolation tasks [4, 3, 5]. These kernels have been successfully employed in various applications, like medical time series prediction [6], arctic coastal erosion forecasting [7], and urban environmental monitoring in sensor networks [8].

However, an SM kernel cannot directly capture correlations between components because it involves only auto-convolution of base components [3]. In this paper we propose a kernel that explicitly incorporates time and phase delay dependencies between components. First, we analyze the presence of statistical dependencies by using posterior variance and covariance of components [9], which are used to give an example motivating the usefulness of modeling dependencies between components.

Next, we introduce a framework for extending SM kernels to include time and phase delay dependencies between components. Specifically, we design a complex-valued Gaussian spectral density which incorporates time delay and phase delay in the frequency domain and transform it to the time domain through an inverse Fourier Transform. Using cross-convolution between a base component and the reversed complex conjugate of another base component, we then construct a complex-valued and positive definite kernel that captures dependencies between components.

Finally, we introduce the so-called learned dependency (see Equation 28), a measure to analyze dependencies between components captured by the proposed kernel. The resulting new kernel, called Spectral Mixture kernel with time and phase delay Dependencies (SMD), contains a time and phase delay cross-dependence term for each pair of components. The number of hyper-parameters is equal to that of SM plus two extra hyper-parameters for time and phase delay. In the proposed framework SMD without cross-dependencies (that is, by only considering auto-convolution of base components) and with zero time and phase delay reduces to the SM kernel.

We show experimentally that explicitly modeling dependencies between components is beneficial in practice. We assess comparatively the performance of SMD on synthetic and real-life datasets. A stochastic variational inference technique is used to perform scalable inference for training a GP on large dataset. Results indicate that SMD is capable to exploit dependence structure in time series and also in a multi-dimensional dataset: it achieves comparable or better performance and smaller uncertainty intervals than various other baselines. Results show that modeling time and phase delay dependencies between components is particularly beneficial for modeling natural phenomena involving little or no influence from human activity, like the monthly river flow extrapolation task, where moon and sun are primarily responsible for the rising and falling of river tidal flows.

The rest of this paper is organized as follows. Background on GP and a summary of related works are given in Section 2. In Section 3 we analyze the statistical dependency between SM components using the framework introduced by [9]. Section 4 introduces our SMD kernel. Section 5 describes the differences between SMD and other kernels. Section 6 and 7 describe hyper-parameters initialization and experiments on synthetic and real world dataset, respectively. Concluding remarks and future work are reported in Section 8.

## 2 Background

In this section we describe Gaussian processes, Spectral Mixture kernels, and related works.

### 2.1 Gaussian Processes

A Gaussian processes (GP) is any distribution over functions  $f(\mathbf{x})$  such that any finite set of function values have a joint Gaussian distribution. A GP model is completely specified by its mean function  $m(\mathbf{x}) = \mathbb{E}(f(\mathbf{x}))$  and covariance function, the latter also called kernel,  $k(\mathbf{x}, \mathbf{x}') = \text{cov}(f(\mathbf{x}), f(\mathbf{x}'))$  [2]. For input vectors  $\mathbf{x}, \mathbf{x}' \in \mathbb{R}^P$ , we have  $f(\mathbf{x}) \sim \mathcal{GP}(m(\mathbf{x}), k(\mathbf{x}, \mathbf{x}'))$ . It is common practice to assume that the mean function is simply zero everywhere, since uncertainty about the mean function can be taken into account by adding an extra term to the kernel [?, cf. e.g.]Rasmussen2006.

The kernel induces a positive definite covariance matrix  $K = k(X, X)$  of the training locations set  $X$ . For a regression task, we can predict the unknown function values  $\tilde{\mathbf{y}}^*$  and their variances  $\mathbb{V}[\tilde{\mathbf{y}}^*]$  (that is, its uncertainty) for test points

$X^*$  using the following key predictive equations for GP regression [2]:

$$\tilde{\mathbf{y}}^* = K^{*\top} (K + \sigma_n^2 I)^{-1} \mathbf{y} \quad (1)$$

$$\mathbb{V}[\tilde{\mathbf{y}}^*] = K^{**} - K^{*\top} (K + \sigma_n^2 I)^{-1} K^* \quad (2)$$

where  $K^{**} = K(X^*, X^*)$ ,  $K^{*\top}$  is the covariance matrix between  $X^*$  and  $X$ , and  $\mathbf{y}$  are the observed values corresponding to  $X$ . Typically, GPs contain free parameters  $\Theta$ , called hyper-parameters, which can be optimized by minimizing the Negative Log Marginal Likelihood (NLML):

$$\begin{aligned} \text{NLML} &= -\log p(\mathbf{y}|X, \Theta) \\ &\propto \underbrace{\frac{1}{2} \mathbf{y}^\top (K + \sigma_n^2 I)^{-1} \mathbf{y}}_{\text{model fit}} + \underbrace{\frac{1}{2} \log |K + \sigma_n^2 I|}_{\text{complexity penalty}} \end{aligned} \quad (3)$$

where  $\sigma_n^2$  is the noise level and NLML is obtained through marginalization over the latent function [2]. This formulation follows directly from the fact that  $\mathbf{y} \sim \mathcal{N}(0, K + \sigma_n^2 I)$ . Smoothness and generalization properties of GPs depend on the kernel function and its hyper-parameters  $\Theta$  [2].

## 2.2 Spectral Mixture Kernels

The SM kernel, here denoted by  $k_{\text{SM}}$ , was introduced by [3]. It is a stationary kernel, meaning that it is invariant to translation of the input. We can therefore write  $k_{\text{SM}}(\mathbf{x}, \mathbf{x}') = k_{\text{SM}}(\tau)$  where  $\tau = \mathbf{x} - \mathbf{x}'$ . Bochner's Theorem shows that the properties of a stationary kernel entirely depend on its spectral densities [10, 11]. This theorem states the following: a complex-valued function  $k$  on  $\mathbb{R}^P$  is the covariance function of a weakly stationary mean square continuous complex-valued random process on  $\mathbb{R}^P$  if and only if it can be represented as

$$k(\tau) = \int_{\mathbb{R}^P} e^{2\pi i \mathbf{s}^\top \tau} \psi(d\mathbf{s}),$$

where  $\psi$  is a positive finite measure. If  $\psi$  has density  $\hat{k}(\mathbf{s})$ , then  $\hat{k}$  is called the spectral density or power spectrum of  $k$ , and  $k$  and  $\hat{k}$  are Fourier transform dual, that is,  $\hat{k}(\mathbf{s}) = \mathcal{F}_{\tau \rightarrow \mathbf{s}}\{k(\tau)\}$  and  $k(\tau) = \mathcal{F}_{\mathbf{s} \rightarrow \tau}^{-1}\{\hat{k}(\mathbf{s})\}$ , where  $\mathcal{F}_{\tau \rightarrow \mathbf{s}}$  and  $\mathcal{F}_{\mathbf{s} \rightarrow \tau}^{-1}$  denote the Fourier Transform (FT) operator and the inverse FT operator, respectively. In the spectral mixture kernel such probability density function is modeled as mixture of  $Q$  Gaussians in the spectral domain. For the SM kernel, the  $i$ -th component in the frequency domain is defined as

$$\hat{k}_{\text{SM}i}(\mathbf{s}) = (\varphi_{\text{SM}i}(\mathbf{s}) + \varphi_{\text{SM}i}(-\mathbf{s}))/2, \quad (4)$$

where

$$\varphi_{\text{SM}i}(\mathbf{s}) = \frac{1}{\sqrt{(2\pi)^P |\Sigma_i|}} \exp\left(-\frac{1}{2}(\mathbf{s} - \boldsymbol{\mu}_i)^\top \Sigma_i^{-1}(\mathbf{s} - \boldsymbol{\mu}_i)\right). \quad (5)$$

Using the inverse FT, the time domain representation of the SM kernel is:

$$k_{\text{SM}}(\tau) = \sum_{i=1}^Q w_i k_{\text{SM}i}(\tau) \quad (6)$$

$$k_{\text{SM}i}(\tau) = \cos(2\pi \tau^\top \boldsymbol{\mu}_i) \prod_{p=1}^P \exp\left(-2\pi^2 \tau^2 \Sigma_i^{(p)}\right), \quad (7)$$

where  $k_{\text{SM}i}$  is the  $i$ -th SM component,  $P$  denotes the input dimension, and  $w_i$ ,  $\boldsymbol{\mu}_i = [\mu_{i,1}, \dots, \mu_{i,P}]$ , and  $\Sigma_i = \text{diag}([\sigma_{i,1}^2, \dots, \sigma_{i,P}^2])$  are the weight, mean, and variance of the  $i$ -th SM component in the frequency domain, respectively. The variance  $\Sigma_i$  can be thought of as an inverse length-scale,  $\boldsymbol{\mu}_i$  as a frequency, and  $w_i$  as a contribution of the  $i$ -th SM component.

The SM kernel does not capture dependencies between components, because it is a linear combination of the  $k_{\text{SM}i}$ 's components (see Equation 6). Therefore its implicit underlying assumption is that such components are mutually independent. One should not confuse the spectral mixture components that make up the spectral density of the SM kernel with the base components of the Fourier Transform (FT): (1) FT components are periodic trigonometric functions, such as sine and cosine functions, while SM kernel components are quasi-periodic Gaussian functions; (2) FT components are orthogonal (i.e. the product of an arbitrary pair of Fourier series components is zero) while the product of two arbitrary SM components is not necessarily equal to zero; (3) the SM component in the frequency domain is a Gaussian function covering wide frequency range while a FT component is just a sharp peak at a single frequency, which is covered by intersection of SM components (e.g., indicating that they share information, see Figure 3).

### 2.3 Related Work

Various kernel functions for GPs have been proposed, such as Squared Exponential (SE), Periodic (PER), and general Matérn (MA). Recently, SM kernels have been proposed by [3]. Additive GPs have been proposed by [9, 12]. These are GP models whose kernel implicitly sums over all possible products of one-dimensional base kernels. Kernel extensions include the spectral mixture product kernel (SMP)  $k_{\text{SMP}}(\tau|\Theta) = \prod_{p=1}^P k_{\text{SM}}(\tau_p|\Theta_p)$  by [5], which uses multi-dimensional SM kernels, and extends the application scope of SM kernels to image data and spatial data. Other interesting families of kernels include non-stationary kernels [13, 14, 4], which are capable to learn input-dependent covariances between inputs. The above mentioned kernels do not explicitly model dependencies between components. Recently we introduced a method to incorporate cross-dependencies between components of an SM kernel but without time and phase delay [15]. To do so we used the convolution theorem.

Here we consider time and phase delay, which requires the use of a more sophisticated approach, involving a complex-valued Gaussian spectral density incorporating time delay and phase delay in the frequency domain, which is then transformed to the time domain through an inverse Fourier Transform. Moreover, here we provide a more extensive experimental comparative assessment, which shows the beneficial effect of considering time and phase delay dependencies.

The problem of expressing structure present in the data being modeled with kernels has been investigated in the context of kernel composition. Notably, [9] introduced a framework for composing kernel structures. A space of kernel structures is defined in terms of sums and products of a small number of base kernel structures. Then automatic search over this space of kernel structures is performed using marginal likelihood as the optimization criterion. Although composing kernels allows one to produce kernels combining several high-level properties, they depend on the choice of base kernel families, composition operators, and search strategy. Instead, here we directly enhance SM kernels by incorporating dependency between components.

Complex-valued functions to model time and phase delay in the spectral density have been previously employed by [16], where multivariate covariance functions are constructed by using a parametric family of complex-valued cross spectral densities and Bochner's Theorem. The proposed kernels are able to model delays among tasks in addition to phase differences. The cross spectral density between two tasks  $i$  and  $j$  is modeled as a complex-valued square exponential (SE) function with delay  $\theta_i - \theta_j$  and phase  $\phi_i - \phi_j$ . In the single task setting we consider (i.e., for  $i = j$ ) such cross spectral densities become equal to zero. So the proposed kernel does not model phase and time delay dependency between components of a kernel in the single task setting.

The posterior variance and covariance of additive components here used in Section 3 to motivate the introduction of our new SMD kernel has been used by [9] to quantify the correlation between additive components of composite kernels.

## 3 Dependencies between SM components

Since the SM kernel is additive, any function  $f$  drawn from a GP with kernel  $k_{\text{SM}}$ , that is,  $f \sim \mathcal{GP}(0, k_{\text{SM}})$ , can be expressed as

$$f = \sum_{i=1}^Q f_i, \quad (8)$$

where  $f_i \sim \mathcal{GP}(0, w_i k_{\text{SM}i})$  (that is, each  $f_i$  is drawn from a GP with kernel  $w_i k_{\text{SM}i}$ ). With a slight abuse of notation we denote by  $\mathbf{f}_i$  also the function values at training locations  $X$ , and by  $\mathbf{f}_i^*$  both the function and the function values at some set of query locations  $X^*$ .

From the additivity of the SM kernel it follows that the  $f_i$ 's are *a priori* independent. Then, by using the formula for Gaussian conditionals we can give the conditional distribution of a GP-distributed function  $\mathbf{f}_i^*$  conditioned on  $\mathbf{f}_i + \mathbf{f}_j$  with  $\mathbf{f}_j$  another GP-distributed function:

$$\mathbf{f}_i^* | \mathbf{f}_{i+j} \sim \mathcal{N}\left(K_i^{*\top} K_{i+j}^{-1} \mathbf{f}_{i+j}, K_i^{**} - K_i^{*\top} K_{i+j}^{-1} K_i^*\right) \quad (9)$$

where  $\mathbf{f}_{i+j} = \mathbf{f}_i + \mathbf{f}_j$  and  $K_{i+j} = K_i + K_j$ . The reader is referred to [9] (Section 2.4.5) for the derivation of these results. The Gaussian conditionals express the models posterior uncertainty about the different components of the signal, integrating over the possible configurations of the other components.

In particular, we have:

$$\mathbb{V}(\mathbf{f}_i^* | \mathbf{f}_i) = K_i^{**} - K_i^{*\top} K_i^{-1} K_i^*, \quad (10)$$

$$\mathbb{V}(\mathbf{f}_i^* | \mathbf{f}_{i+j}) = K_i^{**} - K_i^{*\top} K_{i+j}^{-1} K_i^*. \quad (11)$$

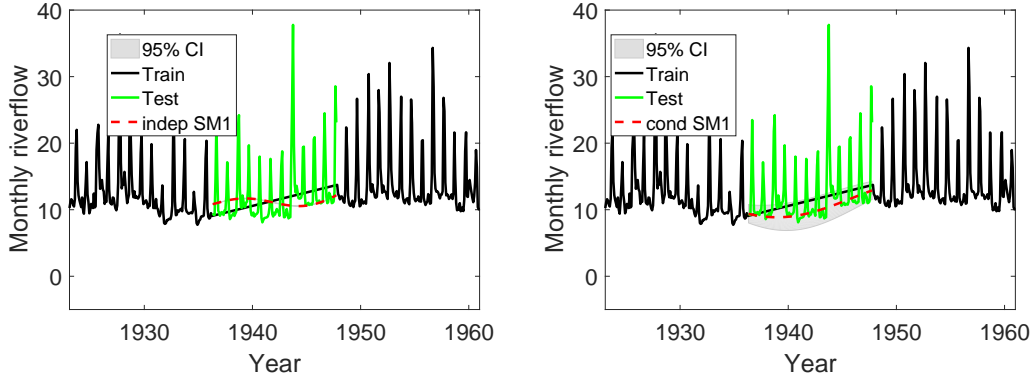


Figure 1: Left: extrapolation results using  $\mathbf{f}_1^* | \mathbf{f}_1$ ; right: extrapolation results using  $\mathbf{f}_1^* | \sum_{i=1}^6 \mathbf{f}_i$

In general when dependencies between components are present we have  $\mathbb{V}(\mathbf{f}_i^* | \mathbf{f}_i) \neq \mathbb{V}(\mathbf{f}_i^* | \mathbf{f}_{i+j})$ . We can also compute the posterior covariance between the height of any two functions, conditioned on their sum [9]:

$$\text{Cov}(\mathbf{f}_i^*, \mathbf{f}_j^* | \mathbf{f}_{i+j}) = -K_i^{*\top} K_{i+j}^{-1} K_j^*. \quad (12)$$

We can use the posterior covariance to show the presence and usefulness of the statistical dependencies between components, as illustrated in the following example. We consider the monthly river flow dataset and experimental setting described in Section 7.2. Figure 1 shows extrapolation results of the first SM component conditioned on different components. Training data, testing data, confidence interval, and extrapolation of SM are shown in black, green, gray, and red dashed line, respectively.

On the left hand side of Figure 1, extrapolation is performed using the hyper-parameters values of the first component obtained by training a GP with  $Q = 6$  components. The right hand side of the figure plots extrapolation results obtained by using the Gaussian conditionals (see Equation (9)). The figure shows that extrapolation results of the first SM component are different between the two above mentioned settings with respect to both trend and confidence interval. In Figure 1, the extrapolation shown in subplot (b) is obtained implicitly using posterior covariance (see Equation (9) and Equation (12)) hence it is significantly different than that shown in subplot (a). The example clearly shows that the posterior covariance between components corrects the predictive trends and increases uncertainty. The beneficial effect of posterior covariance between components is illustrated in the Appendix, where the extrapolation is obtained using all components, that is,  $\sum_{i=1}^6 (\mathbf{f}_i^* | \sum_{i=1}^6 \mathbf{f}_i)$  is compared with  $\sum_{i=1}^6 (\mathbf{f}_i^* | \mathbf{f}_i)$ .

We can use the normalized posterior covariance, here called posterior correlation coefficient, to quantify the presence of statistical dependence:

$$\rho_{ij} = \frac{\text{Cov}(\mathbf{f}_i^*, \mathbf{f}_j^* | \mathbf{f}_i, \mathbf{f}_j)}{(\mathbb{V}(\mathbf{f}_i^* | \mathbf{f}_i, \mathbf{f}_j) \mathbb{V}(\mathbf{f}_j^* | \mathbf{f}_i, \mathbf{f}_j))^{1/2}}. \quad (13)$$

$\rho_{ij}$  can be used as indicator of statistical dependence between components  $i$  and  $j$ : there is no dependence between the  $i$ -th and  $j$ -th SM components if  $\rho_{ij} = 0$ , otherwise there are dependencies. We will use  $\rho_{ij}$  in our experiments.

## 4 Spectral Mixture Kernels with Time and Phase Delay Dependencies

We describe now our approach for incorporating time and phase delay dependencies in SM kernels. First, time delay and phase delay are incorporated into each base component. Next, a so-called SMD cross-component term is constructed by performing cross-convolution between a base component and the reversed complex conjugate of another base component (see Section 4.1). Finally, SMD cross-component terms are used to construct a complex-valued and positive definite kernel representing correlations between base components (see Section 4.2).

By the time shift property, shifting a signal in the time domain amounts to the Fourier transformed signal to be multiplied by a complex exponential in the frequency domain: for any time delayed function  $k_\theta(\tau) = k(\tau - \theta)$ , its Fourier transform is

$$\hat{k}_\theta(\mathbf{s}) = e^{-2\pi\theta\mathbf{s}} \hat{k}(\mathbf{s}), \quad (14)$$

where  $i$  denotes the imaginary number [?, see, e.g.]Bateman1954. Also, the phase delay  $\phi$  in the frequency domain is obtained by a multiplication by  $e^{-2\pi i\phi}$ :

$$\hat{k}_\phi(\mathbf{s}) = e^{-2\pi i\phi} \hat{k}(\mathbf{s}) \quad (15)$$

So in the frequency domain we can directly embed time and phase delay in the  $j$ -th weighted Gaussian component  $w_j\varphi_{\text{SM}_j}(\mathbf{s})$  of a spectral mixture kernel, yielding the following complex-valued function, that we call *time and phase delayed spectral density function*:

$$\hat{k}_{\text{SMD}_j}(\mathbf{s}) = w_j\varphi_{\text{SM}_j}(\mathbf{s})e^{-2\pi i(\boldsymbol{\theta}_j\mathbf{s} + \phi_j)} \quad (16)$$

#### 4.1 Convolution of Time Delayed and Phase Delayed Components

A stationary covariance function  $k(\mathbf{x}, \mathbf{x}')$  can be represented as a convolution form on  $\mathbb{R}^P$  as follows [18, 19, 20]:

$$k(\mathbf{x}, \mathbf{x}') \stackrel{\text{def}}{=} \int_{\mathbb{R}^P} g(\mathbf{u}) g(\tau - \mathbf{u}) d\mathbf{u} = (g * g)(\tau), \quad (17)$$

where  $\tau = \mathbf{x} - \mathbf{x}'$  and  $*$  denotes the convolution operator. Since a convolution in the time domain corresponds to a product in the frequency domain, for SM kernel we obtain

$$w_i\hat{k}_{\text{SM}_i}(\mathbf{s}) = (\hat{g}_{\text{SM}_i}(\mathbf{s}))^2 \quad (18)$$

where  $\hat{g}_{\text{SM}_i}(\mathbf{s})$  is the basis function of the  $i$ -th weighted spectral density. In our setting, we want to model dependencies between components. We could use the cross correlation between components  $f_i \sim \mathcal{GP}(0, w_i k_{\text{SM}_i})$  and  $f_j \sim \mathcal{GP}(0, w_j k_{\text{SM}_j})$ , which is similar in nature to the convolution of two functions  $f_i$  and  $f_j$ , defined as

$$w_i k_{\text{SM}_i}(\tau) \star w_j k_{\text{SM}_j}(\tau) = \mathcal{F}_{s \rightarrow \tau}^{-1} [w_i \varphi_{\text{SM}_i}(\mathbf{s}) \cdot \overline{w_j \varphi_{\text{SM}_j}(\mathbf{s})}] (\tau) \quad (19)$$

where  $\mathcal{F}_{s \rightarrow \tau}^{-1}$ ,  $\star$ , and  $\overline{(\cdot)}$  denote the inverse FT, the cross correlation operator, and the complex conjugate operator, respectively. However, if we use Equation (19) to express cross-dependencies, then we would obtain a kernel that is the inverse Fourier Transform of the squared Gaussian  $w_i^2 \varphi_{\text{SM}_i}^2(\mathbf{s})$ . This would be different from the SM kernel, in particular with a smaller inverse length scale. Therefore we consider the cross correlation between the *base components* of the  $i$ -th and of the  $j$ -th weighted spectral density functions.

In the frequency domain  $w_i\hat{k}_{\text{SM}_i}(\mathbf{s})$  is equal to the square of its base component  $\hat{g}_{\text{SM}_i}(\mathbf{s})$  when  $i = j$  (see Equation (18)), that is, the auto-spectral density of one SM component. So, without time and phase delay, in the frequency domain the cross spectral density term corresponding to the cross correlation of the  $i$ -th and  $j$ -th base components in SM can be defined as follows:

$$\hat{k}_{\text{SMD}, \boldsymbol{\theta}=0, \phi=0}^{i \times j}(\mathbf{s}) = \hat{g}_{\text{SM}_i}(\mathbf{s}) \cdot \overline{\hat{g}_{\text{SM}_j}(\mathbf{s})} \quad (20)$$

The kernel corresponding to this spectral density has been investigated in [15]. Now in order to express cross-dependencies also in the presence of time and phase delay, we consider the base spectral density of each  $\hat{k}_{\text{SMD}_i}(\mathbf{s})$ :

$$\hat{g}_{\text{SMD}_i}(\mathbf{s}) = \sqrt{\hat{k}_{\text{SMD}_i}(\mathbf{s})}. \quad (21)$$

Then in the presence of time and phase delay we can define the cross spectral density term as

$$\begin{aligned} \hat{k}_{\text{SMD}}^{i \times j}(\mathbf{s}) &= \hat{g}_{\text{SMD}_i}(\mathbf{s}) \cdot \overline{\hat{g}_{\text{SMD}_j}(\mathbf{s})} \\ &= w_{ij} (\varphi_{\text{SM}_i}(\mathbf{s}) \varphi_{\text{SM}_j}(\mathbf{s}))^{1/2} \exp(-\pi i (\boldsymbol{\theta}_{ij}\mathbf{s} + \phi_{ij})) \\ &= w_{ij} \underbrace{\left( \frac{\exp(-\frac{1}{2}(\mathbf{s} - \boldsymbol{\mu}_{ij})^\top \Sigma_{ij}^{-1}(\mathbf{s} - \boldsymbol{\mu}_{ij}))}{\sqrt{(2\pi)^P |\Sigma_{ij}|}} \right)}_{\text{normal cross Gaussian spectral density}} \underbrace{\exp\left(-\pi i (\boldsymbol{\theta}_{ij}\mathbf{s} + \phi_{ij})\right)}_{\text{cross time and phase delay}} \end{aligned} \quad (22)$$

with the following parameters:

- cross weight:  $w_{ij} = \sqrt{w_i w_j}$ ,
- cross amplitude:  $a_{ij} = \left| \frac{\sqrt{4\Sigma_i \Sigma_j}}{\Sigma_i + \Sigma_j} \right|^{\frac{1}{2}} \exp\left(-\frac{1}{4}(\boldsymbol{\mu}_i - \boldsymbol{\mu}_j)^\top (\Sigma_i + \Sigma_j)^{-1} (\boldsymbol{\mu}_i - \boldsymbol{\mu}_j)\right)$ ,

- cross mean:  $\boldsymbol{\mu}_{ij} = \frac{\Sigma_i \boldsymbol{\mu}_j + \Sigma_j \boldsymbol{\mu}_i}{\Sigma_i + \Sigma_j}$ ,
- cross covariance:  $\Sigma_{ij} = \frac{2\Sigma_i \Sigma_j}{\Sigma_i + \Sigma_j}$ ,
- cross time delay:  $\boldsymbol{\theta}_{ij} = \boldsymbol{\theta}_i - \boldsymbol{\theta}_j$ ,
- cross phase delay:  $\boldsymbol{\phi}_{ij} = \boldsymbol{\phi}_i - \boldsymbol{\phi}_j$ .

Parameters  $\boldsymbol{\mu}_{ij}$  and  $\Sigma_{ij}$  can be interpreted as frequency and inverse length-scale of the cross-component  $k_{\text{SMD}}^{i \times j}(\tau)$ . Cross amplitude  $a_{ij}$  is a normalization constant which does not depend on  $\mathbf{s}$ . When no cross time and phase delay are considered,  $\hat{k}_{\text{SMD}}^{i \times j}(\mathbf{s})$  reduces to the standard cross Gaussian spectral density term. We can observe that the denser mixture of Gaussian components are, and the closer the weight  $w_{ij}$ , frequency  $\boldsymbol{\mu}_{ij}$ , and scale  $\Sigma_{ij}$  between components in SM are, the higher the cross convolution components contribution in SMD will be.

In the time domain we can define the so-called SMD cross-component (the new term in the proposed SM kernel representing dependency between two components) as

$$k_{\text{SMD}}^{i \times j}(\tau) = \mathcal{F}_{\mathbf{s} \rightarrow \tau}^{-1} \{ \hat{g}_{\text{SMD}_i}(\mathbf{s}) \cdot \overline{\hat{g}_{\text{SMD}_j}(\mathbf{s})} \}, \quad (23)$$

which models time and phase dependencies between SM base components.

## 4.2 Spectral Mixture Kernels with Time and Phase Delay Dependencies

By using inverse Fourier transform on the cross spectral density  $\hat{k}_{\text{SMD}}^{i \times j}(\mathbf{s})$ , if there are  $Q$  components in the SM kernel, by considering the distributivity of the convolution operator, we have

$$\begin{aligned} & \mathcal{F}_{\mathbf{s} \rightarrow \tau}^{-1} \left[ \sum_{i=1}^Q \sum_{j=1}^Q \hat{k}_{\text{SMD}}^{i \times j}(\mathbf{s}) \right] (\tau) \\ &= \sum_{i=1}^Q \sum_{j=1}^Q c_{ij} \exp \left( -\frac{\pi^2}{2} (2\tau - \boldsymbol{\theta}_{ij})^\top \Sigma_{ij} (2\tau - \boldsymbol{\theta}_{ij}) \right) \\ & \quad \times \left( \cos \left( \pi \left( (2\tau - \boldsymbol{\theta}_{ij})^\top \boldsymbol{\mu}_{ij} - \boldsymbol{\phi}_{ij} \right) \right) + i \sin \left( \pi \left( (2\tau - \boldsymbol{\theta}_{ij})^\top \boldsymbol{\mu}_{ij} - \boldsymbol{\phi}_{ij} \right) \right) \right) \end{aligned} \quad (24)$$

where  $c_{ij} = w_{ij} a_{ij}$  is the cross-contribution term incorporating cross weight and cross amplitude, which quantifies the dependency between components  $i$  and  $j$  in SMD.

To show that Equation (24) is a legal kernel we need to demonstrate that it is positive semi-definite. This amounts to demonstrate that its spectral density  $\hat{k}_{\text{SMD}}(\mathbf{s})$  is positive semi-definite [10, 11, 21, 22]. Here, given any finite set of non-zero vectors  $[\mathbf{z}_1, \dots, \mathbf{z}_N]^\top \in \mathbb{C}^{N \times P}$  with complex entries,  $\mathbf{s} \in \mathbb{R}^P$ , we have

$$\begin{aligned} \sum_{n=1}^N \mathbf{z}_n \left( \sum_{i=1}^Q \sum_{j=1}^Q \hat{k}_{\text{SMD}}^{i \times j}(\mathbf{s}) \right) \mathbf{z}_n^\dagger &= \sum_{n=1}^N \left( \mathbf{z}_n \left( \sum_{i=1}^Q \hat{g}_{\text{SMD}_i}(\mathbf{s}) \right) \cdot \left( \sum_{j=1}^Q \overline{\hat{g}_{\text{SMD}_j}(\mathbf{s})} \right) \mathbf{z}_n^\dagger \right) \\ &= \sum_{n=1}^N \left( \left( \sum_{i=1}^Q \mathbf{z}_n \hat{g}_{\text{SMD}_i}(\mathbf{s}) \right) \cdot \left( \sum_{j=1}^Q \overline{\mathbf{z}_n \hat{g}_{\text{SMD}_j}(\mathbf{s})} \right) \right) \\ &= \sum_{n=1}^N \left| \left( \sum_{i=1}^Q \mathbf{z}_n \hat{g}_{\text{SMD}_i}(\mathbf{s}) \right) \right|^2 \geq 0 \end{aligned} \quad (25)$$

where  $\mathbf{z}_n^\dagger$  denotes the conjugate transpose of  $\mathbf{z}_n$ . Thus the sum of cross spectral densities satisfies the positive definite condition. Therefore from Equation (25) it follows that (24) is positive semi-definite. As also mentioned in Section 2.2, by considering the symmetric properties of spectral density, we obtain our new kernel, called Spectral Mixture kernel with time and phase Delay Dependencies (SMD):

$$k_{\text{SMD}}(\tau) = \sum_{i=1}^Q \sum_{j=1}^Q \left[ \overbrace{c_{ij} \exp \left( -\frac{\pi^2}{2} (2\tau - \boldsymbol{\theta}_{ij})^\top \Sigma_{ij} (2\tau - \boldsymbol{\theta}_{ij}) \right)}^{\text{Scaled exponential part}} \times \underbrace{\cos \left( \pi \left( (2\tau - \boldsymbol{\theta}_{ij})^\top \boldsymbol{\mu}_{ij} - \boldsymbol{\phi}_{ij} \right) \right)}_{\text{Periodical cosine part}} \right] \quad (26)$$

From this equation we can see that the SMD kernel is a mixture of periodic cosine kernels, weighted by squared exponentials, like the SM kernel. In contrast to the SM kernel, SMD also includes a cross component term for each of the  $Q^2$  pairs of components. If we do not consider time and phase delay dependencies between different components, the cross components are only based on the cross convolution of ordinary base components in SM. In this case SMD becomes

$$k_{\text{SMD}}(\tau) = \sum_{i=1}^Q \sum_{j=1}^Q c_{ij} \exp(-2\pi^2 \tau^\top \Sigma_{ij} \tau) \cos(2\pi \tau^\top \boldsymbol{\mu}_{ij}). \quad (27)$$

In SMD, each  $(i, j)$  term in Equation (26) with  $i \neq j$ , that is  $k_{\text{SMD}}^{i \times j}(\tau)$ , represents the dependency between components  $i$  and  $j$  captured by our kernel. We use its normalized form

$$\gamma_{ij}(\tau) = \frac{k_{\text{SMD}}^{i \times j}(\tau)}{\sqrt{k_{\text{SMD}}^{i \times i}(\tau) k_{\text{SMD}}^{j \times j}(\tau)}} \quad (28)$$

as a measure of dependency between components represented by the SMD kernel, so that  $\gamma_{ij} = 1$  when  $i = j$ .

## 5 Comparisons Between SMD and Other Kernels

Figure 2 visualizes the differences between SM and SMD, where each connection represents a convolution structure of the kernel. Circle  $q_i$  corresponds to a GP  $f_i$ . The cross connection denotes a cross correlation of GPs  $f_i$  and  $f_j$ . SM only considers auto-convolutions and ignores dependencies between components.

Table 5 illustrates the differences between SMD and other stationary kernels in terms of their hyper-parameters for a  $P$ -dimension input setting. We consider the linear with bias (LIN) kernel, SE, PER, rational quadratic (RQ), MA. More detailed description about these kernels can be found in [1, 2].

The price to pay for the incorporation of time and phase delay in SMD is that the gradient computation for SMD becomes more involved, because additional time and phase delay hyper-parameters between base components are considered. In Table 5,  $\theta_\lambda$ ,  $\theta_f$ ,  $\theta_\ell$ ,  $\theta_{per}$ , and  $\theta_\alpha$  are length-scales of Automatic Relevance Determination (ARD), signal variance, length-scale, period, and mixture scale hyper-parameters, respectively.

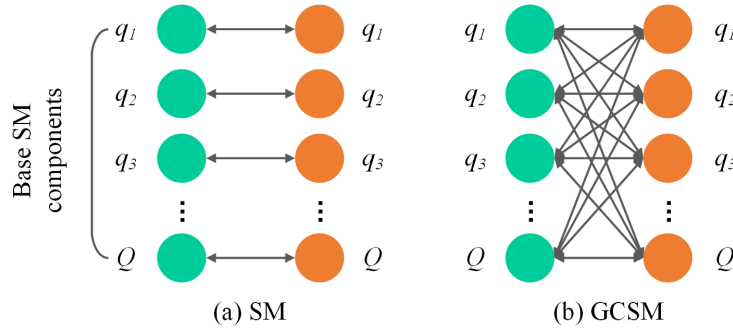


Figure 2: SM and SMD with  $Q$  components. (a) SM models only the auto-convolution between base components. (b) SMD models both auto- and cross-convolution between base components.

We now compare SM and SMD on the same observations from a 1-dimensional input sampled from a  $\mathcal{GP}(0, K_{\text{SM}} + K_{\text{SMD}})$ , using the same initial parameters and noise (see Figure 3 and Figure 4). All SM and SMD covariance, spectral density, and function plots have the same vertical scale.

By considering  $\mathcal{GP}(0, K_{\text{SM}} + K_{\text{SMD}})$  some cross convolution connection pairs (the links between components showed in the right plot in Figure 2) can be cancelled out. We can observe clear differences, in terms of amplitude, peak, and trend between the covariance functions (SM: in dashed red; SMD: in dashed blue). For the corresponding spectral densities, the dependence signal (in magenta) modeled by SMD is also a Gaussian in the frequency domain, which yields a spectral mixture with different magnitude. The posterior distribution and sampling are obtained by conditioning on six observations (in black cross). One can observe that the predictive distribution of SMD has a tighter confidence interval (in blue shadow) than SM (in red shadow).

The plots show the neat contribution of cross-components to the final kernel even with zero time and phase delay. When  $\theta \neq 0$  or  $\phi \neq 0$  the dependency cross-components are shifted and centered at a different position. From this analysis

| Kernel                               | Hyper-parameters                                     | Number of hyper-parameters |
|--------------------------------------|--|----------------------------|
| LIN                                  | $\{\theta_\lambda\}$                                 | $P$                        |
| SE                                   | $\{\theta_f, \theta_\lambda\}$                       | $1 + P$                    |
| PER                                  | $\{\theta_f, \theta_\ell, \theta_{per}\}$            | $2 + P$                    |
| RQ                                   | $\{\theta_f, \theta_\alpha, \theta_\lambda\}$        | $2 + P$                    |
| Matérn                               | $\{\theta_f, \theta_\lambda\}$                       | $1 + P$                    |
| Gabor                                | $\{\theta_{per}, \theta_\lambda\}$                   | $2P$                       |
| SM                                   | $\{w_i, \mu_i, \Sigma_i\}_{i=1}^Q$                   | $(2P + 1) \times Q$        |
| SMD ( $\phi = 0, \theta = 0$ )       | $\{w_i, \mu_i, \Sigma_i\}_{i=1}^Q$                   | $(2P + 1) \times Q$        |
| SMD ( $\phi \neq 0, \theta \neq 0$ ) | $\{w_i, \mu_i, \Sigma_i, \theta_i, \phi_i\}_{i=1}^Q$ | $(4P + 1) \times Q$        |

Table 1: Comparisons between SMD and other popular GP kernels for  $P$ -dimension input in terms of hyper-parameters and number of hyper-parameters.

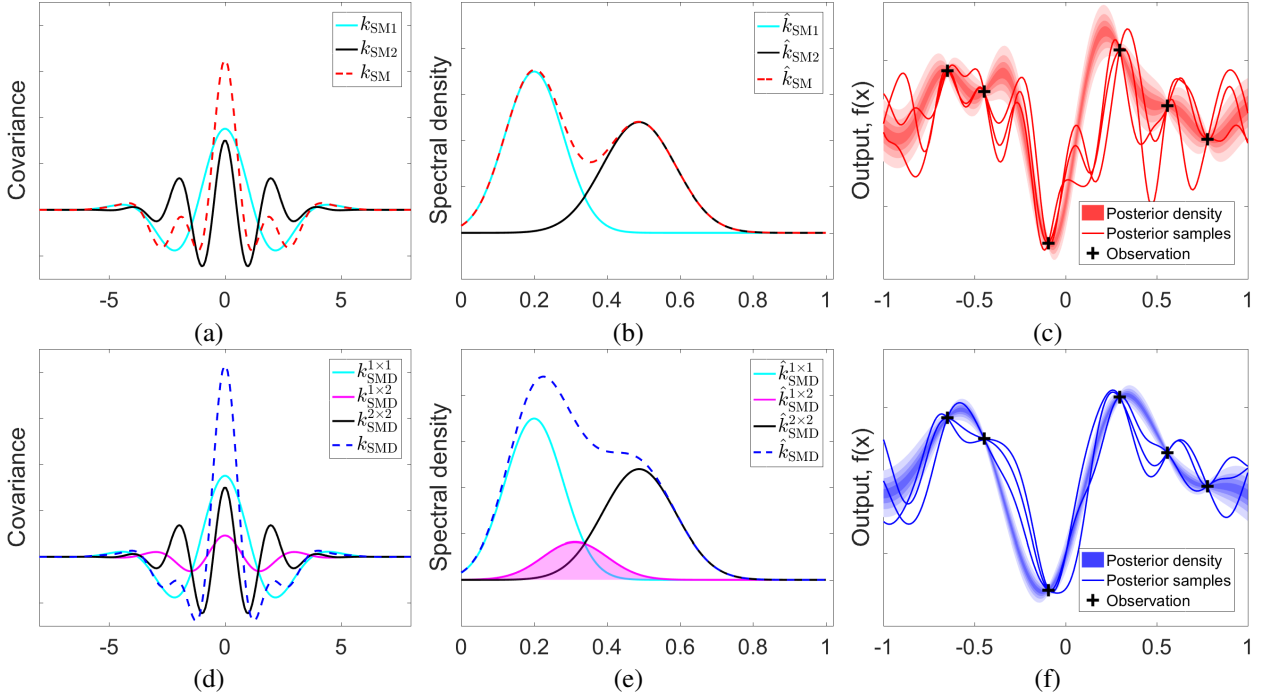


Figure 3: Covariance, spectral density, and posterior functions drawn from GPs with SM ( $Q = 2$ ) and SMD ( $Q = 2$  with zero time and phase delay) kernels conditioning on six samples. In the first row two SM components ( $w_1 k_{SM1}(\tau)$  and  $w_2 k_{SM2}(\tau)$ ) correspond to two solid lines (in cyan and black). In the second row SMD cross-component ( $k_{SMD}(\tau)$ ) (in magenta). SM and SMD plots have the same scale.

and Equation (22) one can observe that the closer the frequency  $\mu_i$ , scale  $\sigma_i$  and weight  $w_i$  between components in SM are, the higher the dependency cross-component's contribution in SMD. On the other hand, according to Equation (26),

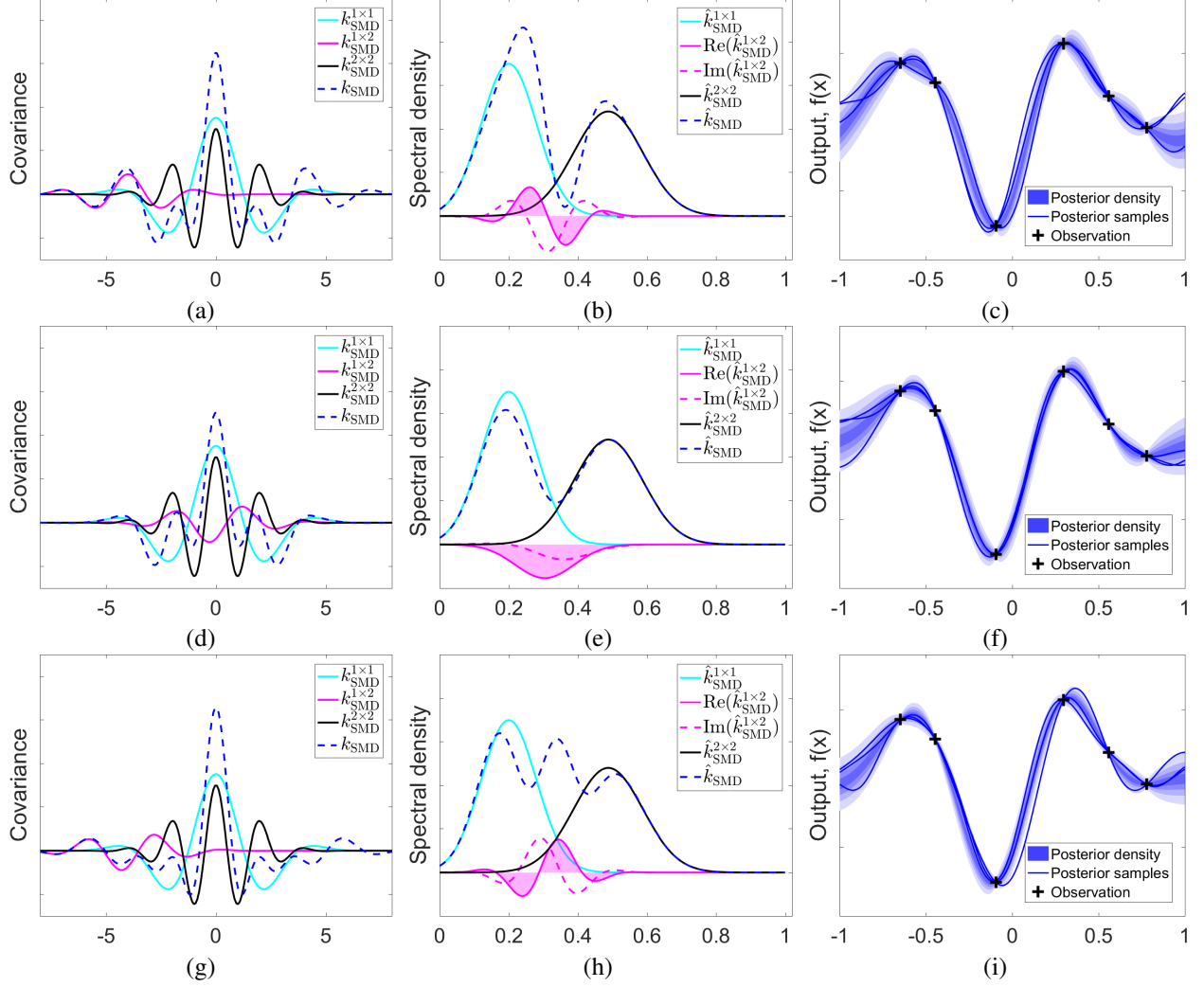


Figure 4: Covariance, spectral density, and posterior functions drawn from GPs with SMD ( $Q = 2$ ) kernels conditioning on six samples. First row: SMD with non-zero time delay and zero phase delay. Second row: zero time delay and non-zero phase delay. Third row: non-zero time and phase delay dependency of cross-components. The samples on the right were obtained using 200 equally-spaced points.

Equation (27), and Equation (6), for diagonal elements of the trained kernel matrix (i.e. with  $\tau = 0$ ), we have

$$k_{\text{SM}}(0) = \sum_{i=1}^Q w_i, \quad (29)$$

$$k_{\text{SMD}}(0) = \sum_{i=1}^Q \sum_{j=1}^Q c_{ij}, \quad (\boldsymbol{\theta} = 0, \boldsymbol{\phi} = 0), \quad (30)$$

$$k_{\text{SMD}}(0) = \sum_{i=1}^Q \sum_{j=1}^Q c_{ij} \exp\left(-\frac{\pi^2}{2} \boldsymbol{\theta}_{ij}^\top \Sigma_{ij} \boldsymbol{\theta}_{ij}\right) \cos\left(-\pi(\boldsymbol{\theta}_{ij} \boldsymbol{\mu}_{ij} + \phi_{ij})\right), \quad (31)$$

$$\gamma_{ij}(0) = a_{ij} \exp\left(-\frac{\pi^2}{2} \boldsymbol{\theta}_{ij}^\top \Sigma_{ij} \boldsymbol{\theta}_{ij}\right) \cos\left(-\pi(\boldsymbol{\theta}_{ij} \boldsymbol{\mu}_{ij} + \phi_{ij})\right). \quad (32)$$

Observe that while the diagonal values of the kernel matrix in SM do not involve the hyper-parameters  $\boldsymbol{\mu}_i$ ,  $\Sigma_i$ , for SMD the diagonal values are affected by all hyper-parameters including time and phase delay.

## 6 Scalable Inference and Hyper-parameters Initialization

For GPs, exact inference has  $\mathcal{O}(n^3)$  computational complexity and  $\mathcal{O}(n^2)$  memory requirements, hence it is prohibitively slow for more than a few thousand datapoints. Computationally expensive steps are: inverting the covariance matrix (i.e.  $(K + \sigma_n^2 I)^{-1}$ , see Equation (1)) and computing the determinant of the covariance (i.e.  $|K + \sigma_n^2 I|$ , see Equation (3)). These issues are addressed by covariance matrix approximation [23, 24, 25] and inference approximation [26, 27].

Here on larger scale datasets, the Synthetic and Abalone datasets, we employ stochastic variational inference (SVI) [26, 27] which provides a generalized framework for combining inducing points  $\mathbf{u}$  and variational inference yielding impressive efficiency and precision. Specifically, SVI approximates the true GP posterior with a GP conditioned on a small set of inducing points  $\mathbf{u}$ . The inducing points  $\mathbf{u}$  as a set of global variables summarise the big training data to perform variational inference. The variational distribution  $P(\mathbf{u}) = \mathcal{N}(\mathbf{u}; \boldsymbol{\mu}_{\mathbf{u}}, \Sigma_{\mathbf{u}})$  with

$$\begin{aligned}\Sigma_{\mathbf{u}} &= K_{\mathbf{u}\mathbf{u}}^{-1} + \sigma_n^{-2} K_{\mathbf{u}\mathbf{u}}^{-1} K_{\mathbf{u}X} K_{\mathbf{u}X}^{\top} K_{\mathbf{u}\mathbf{u}}^{-1} \\ \boldsymbol{\mu}_{\mathbf{u}} &= \sigma_n^{-2} \Sigma_{\mathbf{u}}^{-1} K_{\mathbf{u}\mathbf{u}}^{-1} K_{\mathbf{u}X} \mathbf{y}\end{aligned}\quad (33)$$

gives a variational lower bound  $\mathcal{L}_3(\mathbf{u}; \boldsymbol{\mu}_{\mathbf{u}}, \Sigma_{\mathbf{u}})$ , also called Evidence Lower Bound (ELBO) of the quantity  $p(\mathbf{y}|X)$  [26, 27].

$$\log p(\mathbf{y}|X) \geq \mathcal{L}_3(\mathbf{u}; \boldsymbol{\mu}_{\mathbf{u}}, \Sigma_{\mathbf{u}}) \quad (34)$$

where  $K_{\mathbf{u}X}$  is the SMD covariance between  $\mathbf{u}$  and  $X$  and  $K_{\mathbf{u}\mathbf{u}}$  is the SMD covariance of  $\mathbf{u}$ . From [26], the variational distribution  $\mathcal{N}(\mathbf{u}; \boldsymbol{\mu}_{\mathbf{u}}, \Sigma_{\mathbf{u}})$  contains all the information in the posterior approximation, which represents the distribution on function values at the inducing points  $\mathbf{u}$ . From  $\frac{\partial \mathcal{L}_3}{\partial \boldsymbol{\mu}_{\mathbf{u}}} = 0$  and  $\frac{\partial \mathcal{L}_3}{\partial \Sigma_{\mathbf{u}}} = 0$ , we can obtain an optimal solution of the variational distribution. Thus the posterior distribution [26, 27] of testing point can be written as

$$p(y^*|\mathbf{x}^*, X, Y) = \mathcal{N}(\mathbf{k}_{\mathbf{u}}^* K_{\mathbf{u}\mathbf{u}}^{-1} \boldsymbol{\mu}_{\mathbf{u}}, h^{**} + \mathbf{k}_{\mathbf{u}}^{*\top} (K_{\mathbf{u}\mathbf{u}}^{-1} \Sigma_{\mathbf{u}} K_{\mathbf{u}\mathbf{u}}^{-1} - K_{\mathbf{u}\mathbf{u}}^{-1}) \mathbf{k}_{\mathbf{u}}^*) \quad (35)$$

where  $\mathbf{k}_{\mathbf{u}}^*$  is the SMD covariance vector between  $\mathbf{u}$  and test point  $\mathbf{x}^*$ . Here the complexity of SVI is  $\mathcal{O}(m^3)$  where  $m$  is the number of inducing points. In our experiment with a large multi-dimensional dataset (see Section 7.7) we set  $m = 500$ .

### 6.1 Hyper-parameter Initialization

In the experiments described in the next section, we use the empirical spectral densities to initialize the hyper-parameters, as recommend in [3, 13]. Different from these works, we apply a Blackman window function to the training data to improve the quality of empirical spectral densities, e.g. the signal to noise ratio (SNR), and to more easily discover certain characteristics of the signal, e.g. magnitude and frequency. We consider the windowed empirical spectral densities  $\mathbf{s}$  as derived from the data, and then apply a Bayesian Gaussian mixture model (GMM) in order to get the  $Q$  cluster centers of the Gaussian spectral densities [13].

$$p(\tilde{\Theta}|\mathbf{s}) = \sum_{i=1}^Q \tilde{w}_i \mathcal{N}(\tilde{\boldsymbol{\mu}}_i, \tilde{\Sigma}_i) \quad (36)$$

We use the Expectation Maximization algorithm [28] to estimate the parameters  $\tilde{w}_i$ ,  $\tilde{\boldsymbol{\mu}}_i$ , and  $\tilde{\Sigma}_i$ . The results are used as initial values of  $w_i$ ,  $\boldsymbol{\mu}_i$ , and  $\Sigma_i$ , respectively. For all kernels we select the hyper-parameters with lowest NLML over 10 initialization trials. The selected hyper-parameters are then used for GP optimization to perform extrapolation.

## 7 Experiments

We comparatively assess the performance of SMD on synthetic and real-world datasets. The first experiment on synthetic data aims to illustrate the beneficial effect of directly modeling phase and delay dependencies. Next, we compare SMD with ordinary SM for prediction tasks on six real-life datasets: the monthly river flow, yearly sunspot, and the larger multidimensional abalone dataset, as well as three benchmark datasets often used in previous works, namely the monthly average atmospheric CO<sub>2</sub> concentrations [2, 29], the monthly ozone concentrations, and the air revenue passenger miles dataset.

The first three experiments with real-life data illustrate comparatively the capability of GPs with the considered kernels to model irregular long term increasing trends. The river flow and the sunspot datasets are generated from an underlying

natural phenomenon that involves limited or no human activity. They contain complex dependencies in their patterns due to physical interference in connection with the relative orbital position of solar planets. While the CO<sub>2</sub> concentrations, the monthly ozone concentrations, and the air revenue passenger miles datasets are related to human activity and contain less complicated time and phase delayed dependency patterns.

We use the Gaussian conditionals introduced in Section 3 to show the role of the posterior covariance in the extrapolation of each component. We use Mean Squared Error ( $MSE = \frac{1}{n} \sum_{i=1}^n (y_i - \tilde{y}_i)^2$ ) as the performance metric for all tasks. The 95% confidence interval (instead of, e.g., error bar) is used to quantify uncertainty (see Equation (2)). In addition to these performance metrics, we also consider the posterior correlation  $\rho_{ij}$  (see Equation (13)) of SM and the learned dependency  $\gamma_{ij}$  (see Equation (28)) of the SMD variant with best MSE performance to show the underlying statistical dependency between SM components and dependency learned by SMD, respectively.

As baselines for comparison we consider the popular kernels implemented in the GPML toolbox [2]: LIN, SE, polynomial (Poly), PER, RQ, MA, Gabor, fractional Brownian motion covariance (FBM), underdamped linear Langevin process covariance (ULL), neural network (NN) and SM kernels. We consider also the recent Non-stationary Spectral Mixtute kernel (NSM) introduced by [4].

For each dataset the same number  $Q$  of components is used for SM, NSM and SMD. For the considered multidimensional dataset, we use ARD for other baseline kernels to remove irrelevant input. Note that the FBM, ULL and NSM kernels are not directly applicable to multidimensional dataset ( $P > 2$ ). In all plots, training, testing, SM, SMD and confidence interval are respectively in black, green, red, blue, and gray shadow. For the Large Scale Multidimensional and for the artificial dataset we use the GPflow toolbox [30] and for the other datasets we use GPML [1]. For SMD, we calculate the gradient of the parameters using an analytical derivative technique. We use LBFGS to optimize the hyper-parameters of the kernel.

### 7.1 Synthetic Signal with Dependency Structure

We illustrate the capability of SMD to capture time and phase delay dependencies using an artificial dataset. We sample a signal from the following GP with a hybrid kernel structure consisting of the sum of an SMD kernel with dependent structure and an SM kernel with independent structure, both kernels with  $Q = 2$  components:

$$f(x) \sim \mathcal{GP}(0, K_{SMD}(\theta \neq 0, \phi \neq 0) + K_{SM}). \quad (37)$$

We generate a normal time series of length 300 in the interval  $[-10, 10]$  and add some noise into it (see Figure 5). In this experiment we remove the middle 40% of the signal and consider it as missing testing data (in green). The rest of the signal forms the training data (in black). SMD and SM are configured with the same number of components  $Q = 5$  for all experiments and with the same initial values for the hyper-parameters  $w_i, \mu_i, \sigma_i^2$ . The other parameters of  $k_{SMD}, \theta_i$  and  $\phi_i$ , are initialized randomly.

Results can be summarized as follows. The difference in performance between SMD and SM is neat in terms of fitting and uncertainty. SMD is capable to learn the hybrid covariance structure well. For SM (in dashed red) it is more difficult to recognize such dependent structure and to extrapolate the missing block. SMD yields better prediction and smoother confidence intervals than SM (see Figure 5). Overall, this experiment indicates the capability of SMD to correctly capture dependent patterns of the generative signal without any prior information, and achieves lowest MSE (see Tables 2 and 3). While the NLML of SMD is relatively large at 185.78. As a result of introducing time and phase delay simultaneously in the sampling kernel, here GPs of SMD with no time and phase delays, only time delay, and only phase delay are also unable to extrapolate the missing block well.

### 7.2 Confident Extrapolation of Monthly River Flow

The so-called monthly river flow dataset contains patterns related to time and phase with variability over the period of recording. Especially the moon and sun are primarily responsible for the rising and falling of river tidal flows which are delayed and augmented by their gravity and resonances. The mean monthly river flow in Madison river near west Yellow-stone is the average flow from 1923 to 1960 [31]. Empirical analysis [31] shows various characteristics of this flow data experiment: short term monthly variations, medium term seasonal patterns and non-strict periodic long term trend related to relative position of moon and sun, and some white noises.

As such the monthly river flow involves limited influence from human activity and contains complicated patterns (see Figure 6). There are multiple short term, medium-term and long term trends containing time and phase delay in the monthly river flow time series because the appearance time of flow peak is not periodical and its amplitude is always irregular. There are 456 values in the time series. Here 30% of the data, the long range middle part, was removed as

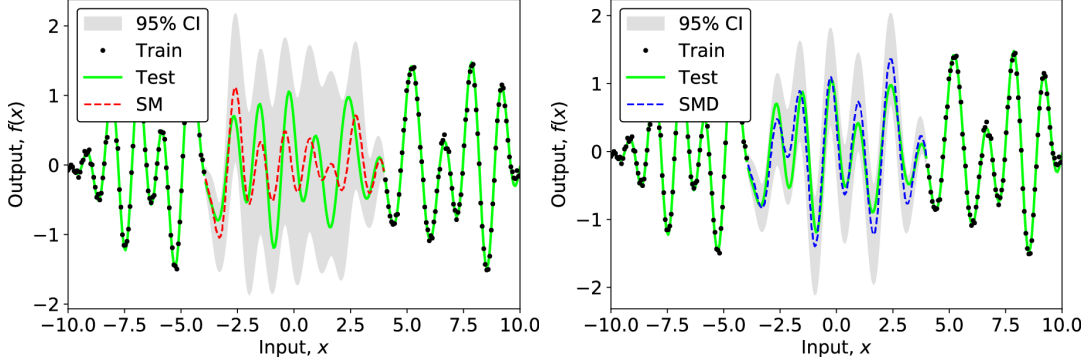


Figure 5: Performance of SM (left) and SMD (right) on a synthetic signal. The testing data is the middle part (40%) of the signal.

testing. While the rest of data was used for training. We use  $Q = 6$  components. Hyper-parameters  $\mu, \Sigma$  are initialized through Bayesian GMM for both SMD and SM, while  $\theta$  and  $\phi$  are randomly initialized in  $k_{SMD}$ .

Results indicate that both SMD and SM can extrapolate the missing month river flow well, with SMD achieving better performance and stronger confidence. Using the same number of components  $Q$ , SMD is in general more effective in modeling the complex patterns occurring in this data (see Tables 2 and 3, and Figure 6).

Overall, results of this experiment clearly show that dependency structure is helpful for extrapolation. Figure 7 (zoom in) shows the posterior correlation  $\rho_{ij}$  of SM kernel and the learned dependency  $\gamma_{ij}$  of SMD. The texture of these plots indicate how components are correlated (negatively or positively). In SM kernel, posterior correlations  $\rho_{24}, \rho_{25},$  and  $\rho_{45}$  of SM components 2, 4, and 5 are evident, indicating the presence of statistical dependency between SM components. For SMD, the values of  $\gamma_{23}, \gamma_{25}, \gamma_{35}$  clearly show that dependencies are captured by this kernel. Note that there is no correspondence between SM and SMD components due to their separate optimization. We can also observe the presence of both positive and negative dependencies, for different values of  $\tau$ , showing the variability of dependencies.

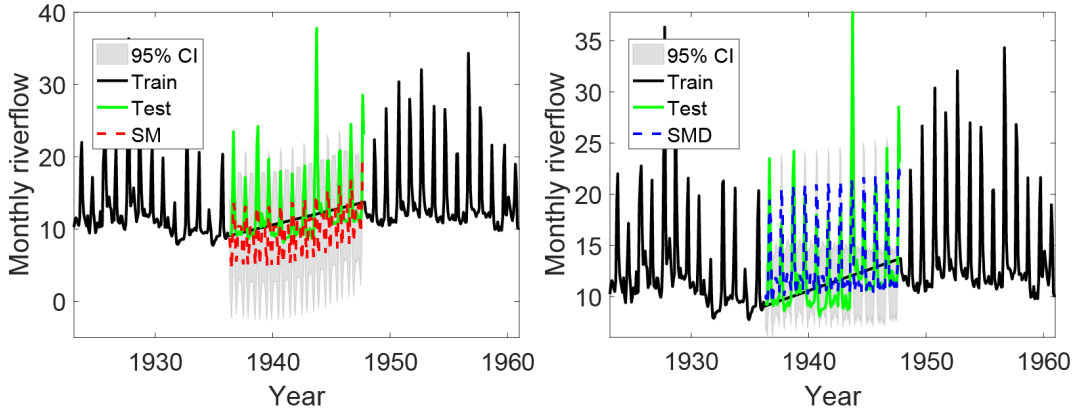


Figure 6: Performance of GP with SM (left) and SMD (right) kernel on the monthly river flow dataset.

### 7.3 Joint Interpolation and Extrapolation of Yearly Sunspot

In this experiment we perform interpolation and extrapolation simultaneously. We consider the yearly sunspot number dataset <sup>1</sup> collected between 1700 and 2014. The historical evolution of yearly sunspot could help to understand spatial magnetic field environment change affected by the Sun activities. The yearly sunspot number was obtained by taking a simple arithmetic mean of the daily total sunspot number over all days of each year. Sunspots appear as spots darker than the surrounding areas on the Sun’s photosphere [32]. They usually have lower surface temperature in contrast to the areas around them. A sunspot has unstable lasting period: the average number of sunspots that is monitored goes up

<sup>1</sup><http://www.sidc.be/silso/infosntotyearly>

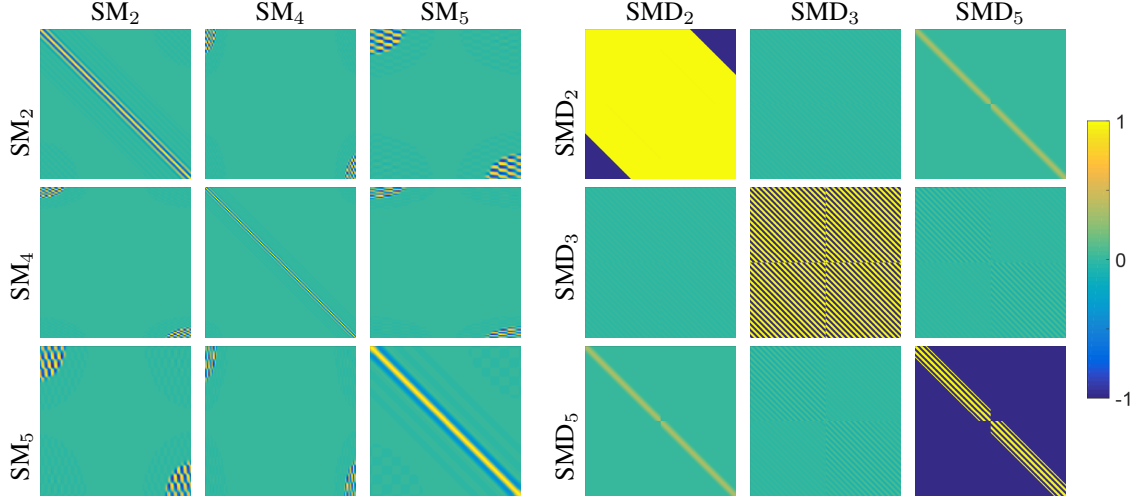


Figure 7: Left: posterior correlations  $\rho_{ij}$  for the SM kernel; Right: learned dependencies  $\gamma_{ij}$  for the SMD kernel.

and down with a quasi-period. There are dependencies between patterns of sunspot, caused by some physical type of interference. This is another example of data generated by a natural process involving limited human activity. As shown in Figure 8, patterns in yearly sunspot contain various irregular peaks over the 315 years. The peak values indicate large variations.

There are 315 values in the time series. We use the last 10% of the data as extrapolation testing dataset, and randomly sample 20% of the original data from the first 90% of the yearly sunspot as interpolation testing dataset. The rest 70% of the data was used for training. Note that the training data is not equally sampled due to the presence of missing values to be interpolated. Therefore here the hyper-parameter initialization is not effective because the Fourier transform does not favor the unequally sampled training data. Therefore in this situation We use random initialization. Time and phase delay in SMD are also randomly initialized. We consider  $Q = 6$  components for both SMD and SM.

Results indicate that both SMD and SM are able to interpolate missing values well with a small confidence interval. However, for the extrapolation part of the task SMD achieves better performance with better confidence (see Tables 2 and 3, and Figure 8).

From Figure 9 we can see that the posterior  $f_1^* | \sum_{i=6}^6 f_i$  conditioned on the sum of all SM components, makes use of posterior covariance between components, it shifts the posterior  $f_1^* | f_1$  and increases its uncertainty. With this experimental result, using the same number of components  $Q = 6$ , SMD can perform interpolation and extrapolation simultaneously well for incomplete signals due to modeling dependent structure.

The left part of Figure 10 shows high posterior correlation coefficient values  $\rho_{12}$ ,  $\rho_{15}$ , and  $\rho_{25}$  indicating the presence of statistical dependency between SM components. Also, Figure 10 (right part) shows SMD has learned dependencies between components, as indicated by the high values of  $\gamma_{12}$ ,  $\gamma_{15}$ , and  $\gamma_{25}$ .

## 7.4 Long Range Extrapolating of CO<sub>2</sub> Concentration

The monthly average atmospheric CO<sub>2</sub> concentration dataset (cf. e.g. [2]) is a popular benchmark used to show the advantage and flexibility of GPs due to multiple patterns with different scales in the data, such as long-term, seasonal and short-term trends. The dataset was collected at the Mauna Loa Observatory, Hawaii, between 1958 and 2003. We use 40% of the location points as training data and the rest 60% as testing data. For both SMD and SM we consider  $Q = 10$  components. The Gaussian mixture of the empirical spectral densities is considered to initialize the hyper-parameters.

Figure 11 shows that SMD (in dashed blue) is better than ordinary SM (in red) in terms of predictive mean and variance. Moreover, SMD yields a smaller confidence interval than SM. Unlike SM, SMD does not overestimate the long-term trend. Results in Tables 2 and 3 show best performance achieved by SMD, with a beneficial effect of phase delay.

As for the analysis of the posterior correlation and learned dependency, evidence of posterior positive and negative correlations  $\rho_{ij}$  can be observed for SM components (3, 4, 7) (left subplot in Figure 13). The right plot in Figure 13 shows clear evidence of learned dependency  $\gamma_{ij}$  for SMD components (2, 3, 4). Here we only show three components with most evident dependency. Note that there is no correspondence between SMD components and SM components

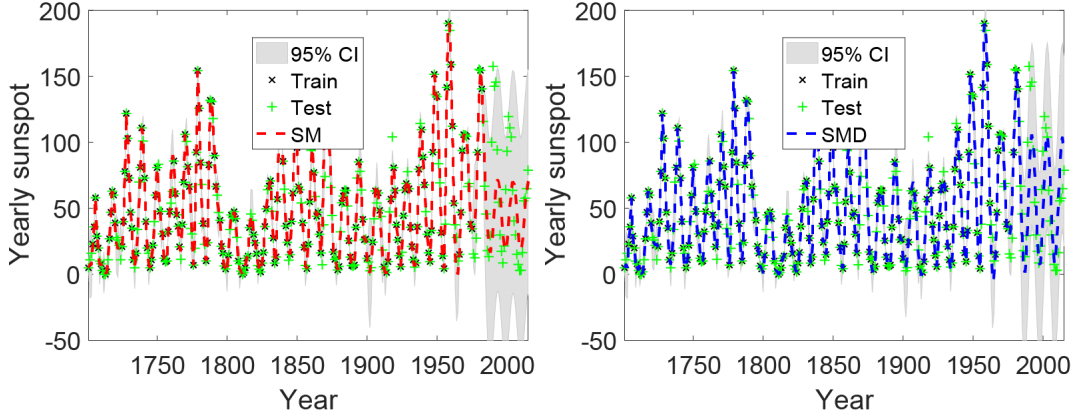


Figure 8: Performance of a GP with SM (left) and SMD (right) kernel on the yearly sunspot dataset.

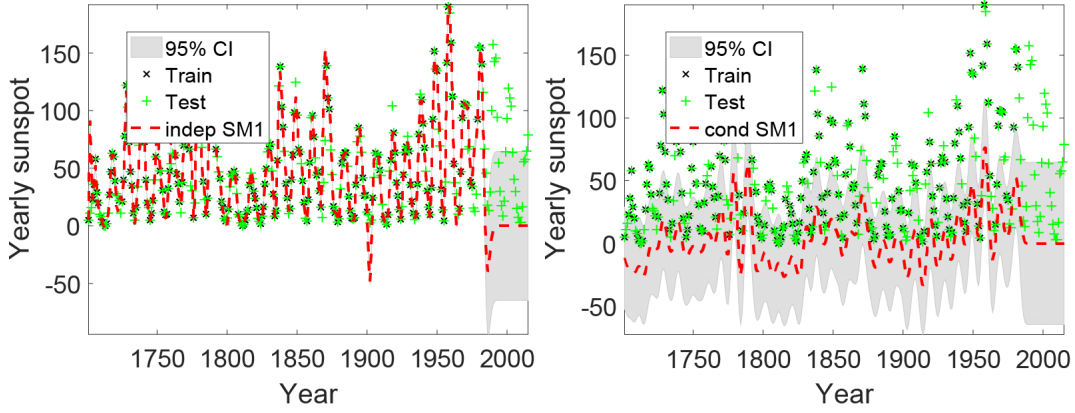


Figure 9: Left: extrapolation results using  $f_1^* | f_1$ ; right: extrapolation results using Gaussian conditionals  $f_1^* | \sum_{i=6}^6 f_i$ .

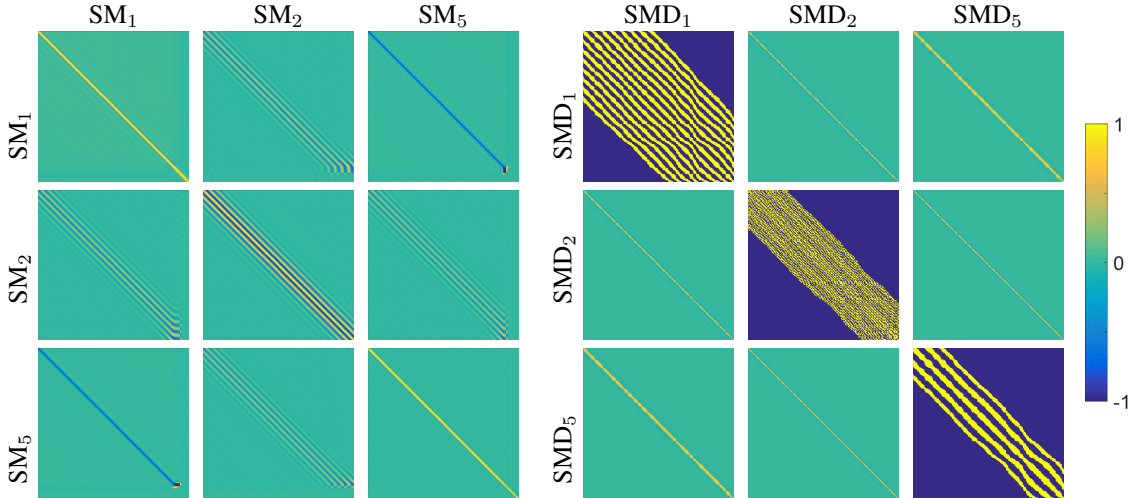


Figure 10: Left: posterior correlations  $\rho_{ij}$  in SM; Right: learned dependencies  $\gamma_{ij}$  in SMD.

because SMD and SM are trained separately. The stripes in the diagonal position of the right subplot show periodical information of the components due to the root of squared form of denominator  $k_{SM_i}$  when  $i = j$  (see Equation 28).

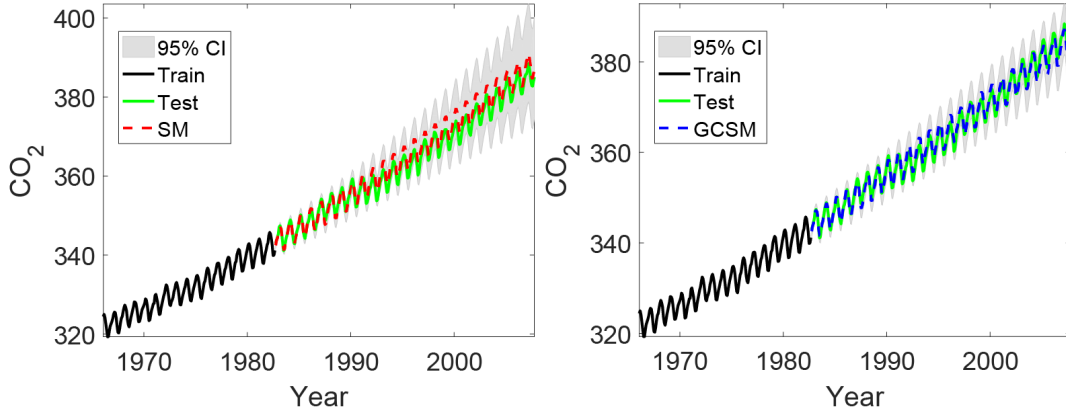


Figure 11: Performance of SM (left) and SMD (right) on the CO<sub>2</sub> concentration dataset.

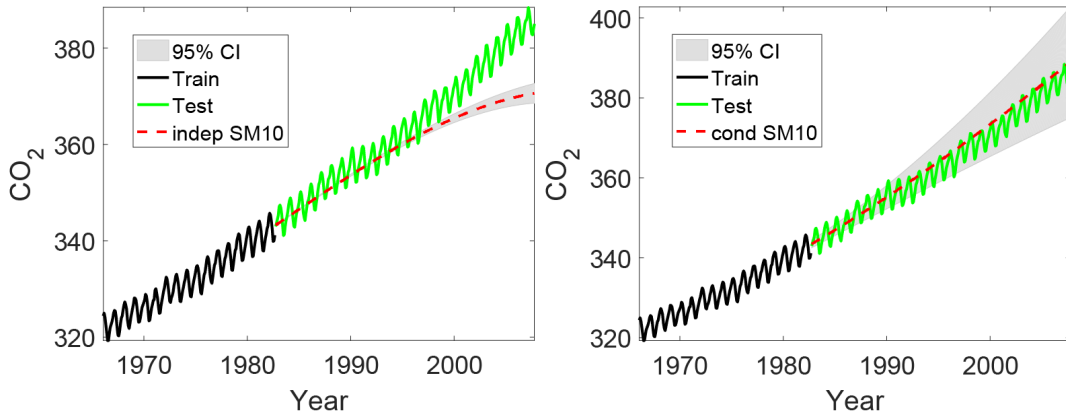


Figure 12: Left: extrapolation results using  $f_{10}^*|f_{10}$ ; right: extrapolation results using Gaussian conditionals  $f_{10}^*|\sum_{i=1}^{10} f_i$

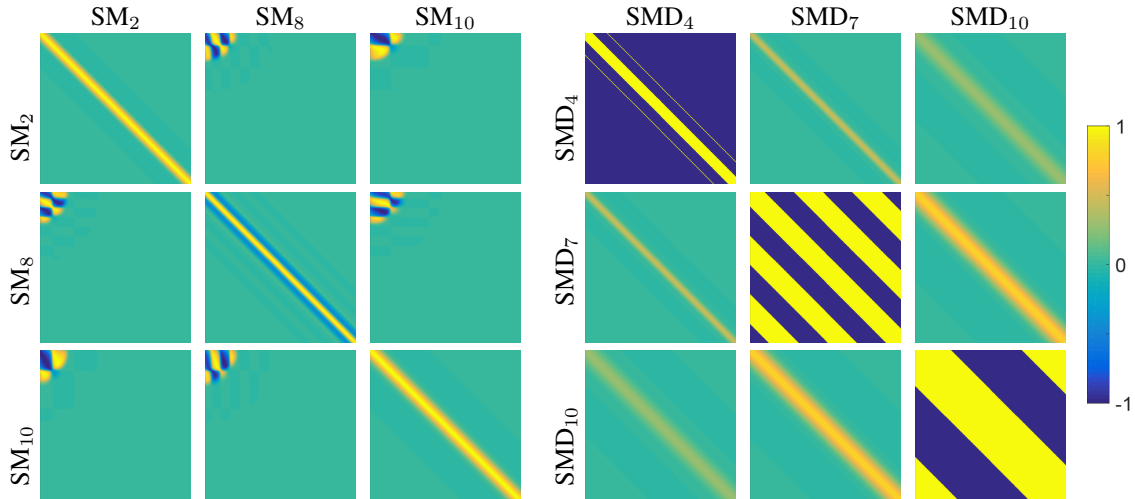


Figure 13: Left: posterior correlations  $\rho_{ij}$  in SM; Right: learned dependencies  $\gamma_{ij}$  in SMD.

Here the SMD with only phase delay has the lowest NLML (at 54.39), while the NLML of SM (at 62.09) is a little bit smaller than that of the other SMD variants.

### 7.5 Modeling Irregular Ozone Concentration Peaks

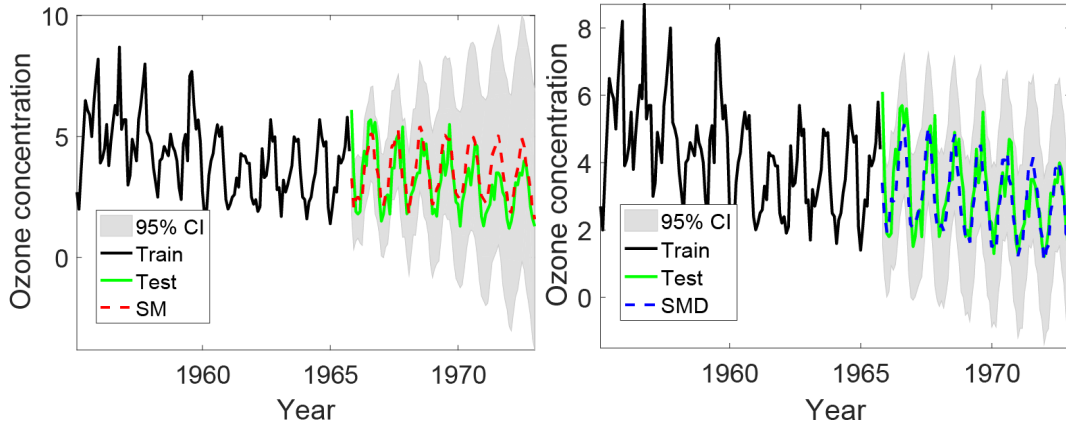


Figure 14: Performance of SM (left) and SMD (right) on the ozone concentration dataset.

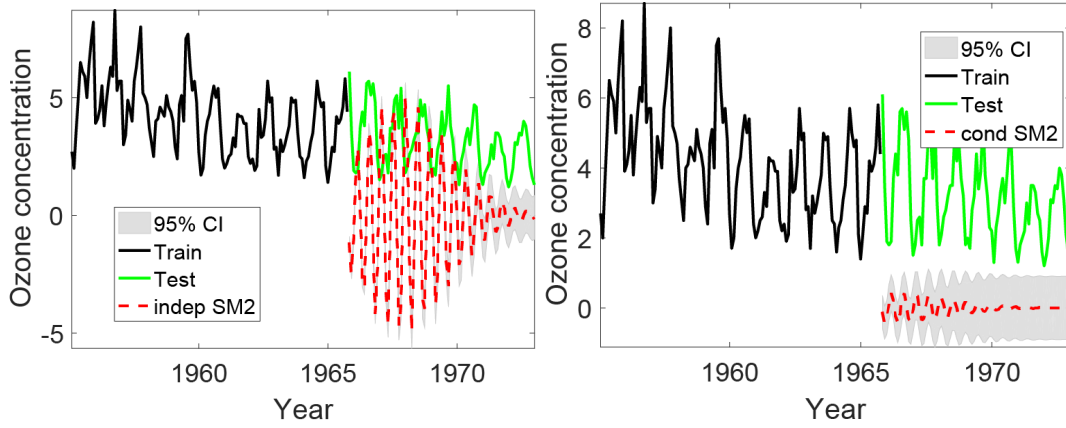


Figure 15: Left: extrapolation results using  $f_2^*|f_2$ ; right: extrapolation results using  $f_2^*|\sum_{i=1}^{10} f_i$

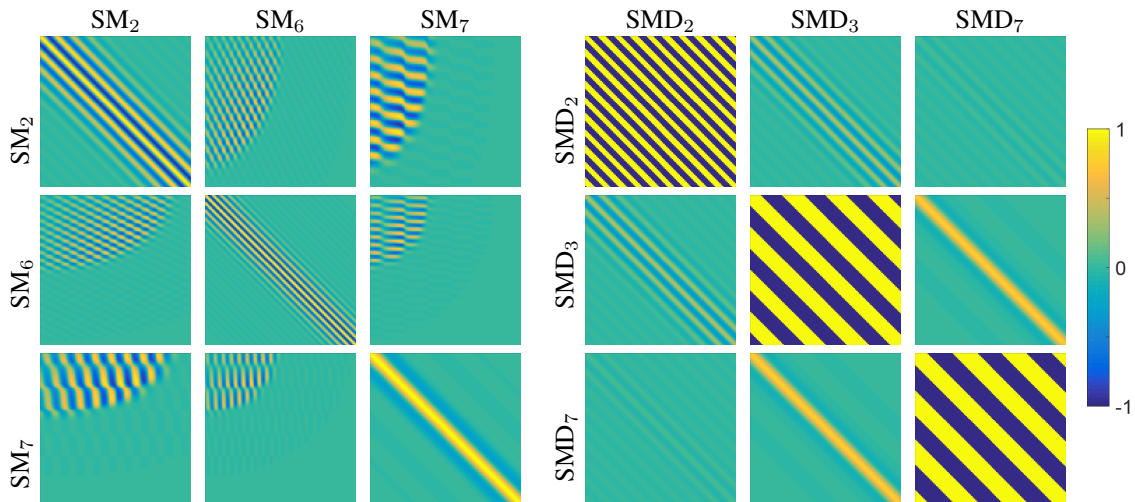


Figure 16: Left: posterior correlations  $\rho_{ij}$  in SM; Right: learned dependencies  $\gamma_{ij}$  in SMD.

We consider now the monthly ozone concentration dataset (216 fact values) collected at Downtown L. A. in the time range January 1955 - December 1972. This dataset has different characteristics than the CO<sub>2</sub> concentration one, namely a gradual long term downtrend and irregular peak values in the training data, which are much higher than those in the testing data (the last part of the time series, see below). These characteristics make extrapolation a challenging task.

Here we use the first 60% of observations for training, and the rest (40%) for testing (shown in black and green in Figure 14, respectively). We consider  $Q = 10$  components for both kernels and the same hyper-parameter initialization (see Section 6.1).

Figure 14 shows that the ozone concentration signal has a long term decreasing tendency while the training part has a relatively stable evolution. Here SM fails to discover such long term decreasing tendency and overestimates the future trend with low confidence. Instead, SMD is able to confidently capture the long term decreasing tendency. These results substantiate the beneficial effect of using dependency cross-components for correcting overestimation and for reducing predictive uncertainty.

Results in Tables 2 and 3 show that on this dataset SMD consistently achieves a lower MSE compared with SM and other baselines. Figure 16 show posterior correlation (left plot) and learned dependency (right plot), The texture of the posterior correlation  $\rho_{ij}$  among SM components (2, 6, 7) demonstrates a more complicated posterior correlation between these components than that of the previous experiment. The learned dependency  $\gamma_{ij}$  is evident for SMD components (2, 3, 7). From Table 3, SMD with no time and phase delay has the best performance, so the plots of extrapolation and learned dependency are based on this SMD.

### 7.6 Modeling Accidental Interfered Air Revenue Passenger Miles

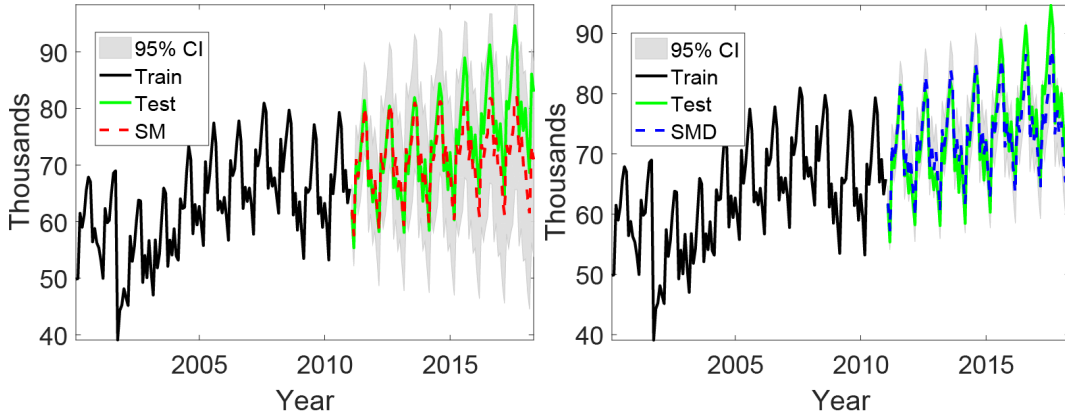


Figure 17: Performance of SM (left) and SMD (right) on air revenue passenger miles.

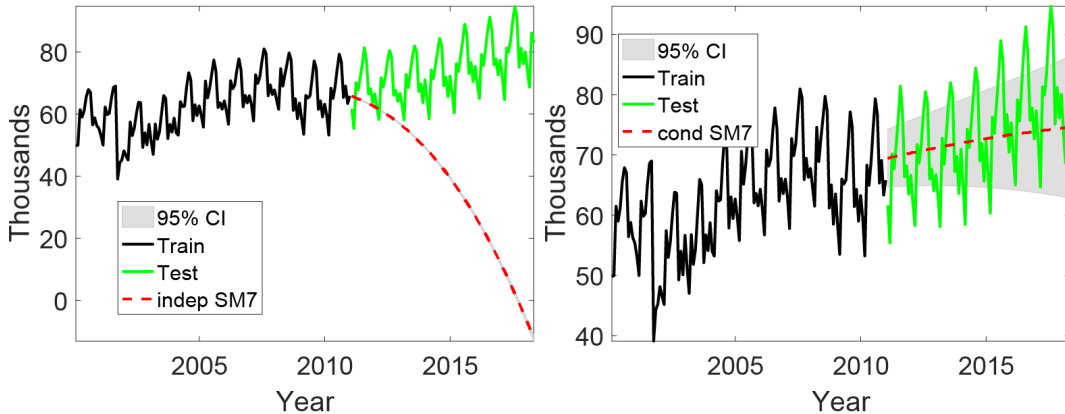


Figure 18: Left: extrapolation results using  $f_7^* | f_7$ ; right: extrapolation results using  $f_7^* | \sum_{i=1}^{10} f_i$

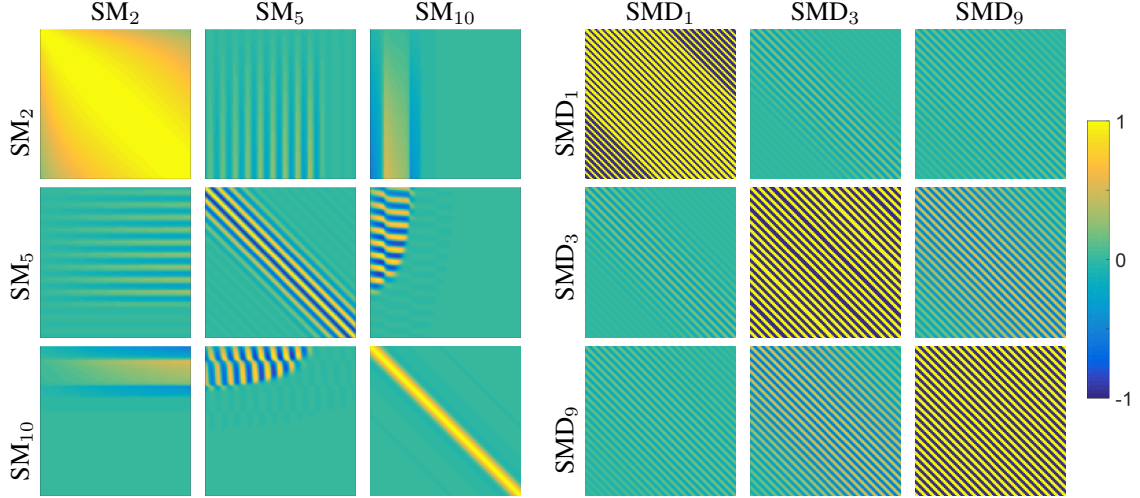


Figure 19: Left: posterior correlations  $\rho_{ij}$  in SM; Right: learned dependencies  $\gamma_{ij}$  in SMD.

In this experiment we consider another challenging extrapolation task, using the air revenue passenger miles <sup>2</sup> with time range Jan 2000 - Apr 2018, monthly collected by the U.S. Bureau of Transportation Statistics. Given 60% recordings at the beginning of the time series, we wish to extrapolate the remaining observations (40%). The challenge here is the presence of long term oscillation tendency in the training observations which is not present in the testing data. As shown in Figure 17, even if at the beginning (in 2001) there seems to be a decreasing trend due to 911 Attack and since 2010 was known as a disappointing year of safety, there is a positive trend as a result of a boosting of the airline market and extensive globalization.

Results in Tables 2 and 3 show that on this dataset SMD consistently achieves a lower MSE compared with SM and other baselines. In particular, kernels such as SE, Periodic and Matérn 5/2 have a poor performance on this extrapolation task. In Figure 19, the left plot shows the posterior correlation coefficient  $\rho_{ij}$  between SM components 2, 5, and 10. We can observe that the posterior covariance of SM components has more complicated behaviors demonstrated by the textures. The right subplot shows the learned dependency  $\gamma_{ij}$  between SMD components 1, 3, and 9. As shown in Table 3, SMD achieves good performance also with zero time and phase delay also has the best performance, which means the dependency are not strongly time and phase delayed.

### 7.7 Prediction with Large Scale Multidimensional Data

So far we have conducted experiments on extrapolation tasks using time series with diverse characteristics. We now consider a prediction task using a larger multidimensional dataset, the Abalone dataset <sup>3</sup>.

This dataset consists of 4177 instances with 8 attributes: Sex, Length, Diameter, Height, Whole weight, Shucked weight, Viscera weight, and Shell weight. The goal is to predict the age of an abalone from physical measurements. Abalone’s age is measured by cutting the shell through the cone, staining it, and counting the number of rings through a microscope. Thus the task is to predict the number of rings from the above mentioned attributes.

We use the first 3377 instances as training data and the remaining 800 as testing data. For both SMD and SM we used  $Q = 5$  components. Recall that we set the number of inducing points  $m = 500$  in SVI. SMD and SM use the same hyper-parameters initialization, as described in Section 6.1. Here components are multivariate Gaussian distributions in the frequency domain. Results in Tables 2 and 3 show that also on this type of task SMD very good performance, with lower MSE than SM.

### 7.8 Discussion

On the Riverflow and Sunspot datasets, results in Tables 2 and 3 demonstrate that SMD ( $\theta \neq 0, \phi \neq 0$ ) performs better than the other SMDs variants ( $\theta = 0$  or  $\phi = 0$ ). These datasets consist of recorded measurements from natural phenomena with little intervention of human activity. They contain physical patterns involving some form of

<sup>2</sup><https://fred.stlouisfed.org/series/AIRRPMTSI>

<sup>3</sup><http://archive.ics.uci.edu/ml/datasets/abalone>

Table 2: Performances of baselines in terms of MSE.

| Kernel | Synthetic | Riverflow | Sunspot | CO <sub>2</sub> | Ozone | Air     | Abalone |
|--------|-----------|-----------|---------|-----------------|-------|---------|---------|
| LIN    | 0.32      | 21.59     | 1544.99 | 39.09           | 1.86  | 57.64   | 10.93   |
| SE     | 0.31      | 161.85    | 649.39  | 128502.50       | 10.40 | 4967.18 | 8.14    |
| Poly   | 0.32      | 172.00    | 1698.85 | 132369.70       | 11.36 | 5535.81 | 6.30    |
| PER    | 0.35      | 17.04     | 1561.78 | 53.37           | 3.87  | 276.07  | 7.98    |
| RQ     | 0.31      | 21.13     | 278.31  | 985.39          | 1.86  | 168.33  | 5.38    |
| MA     | 0.32      | 159.35    | 574.29  | 110735.30       | 9.83  | 4711.33 | 7.52    |
| Gabor  | 0.31      | 21.16     | 4055.16 | 131931.30       | 2.09  | 5535.84 | 4.80    |
| FBM    | 0.49      | 20.67     | 6626.69 | 193.18          | 2.56  | 172.01  | --      |
| ULL    | 0.26      | 70.52     | 489.16  | 117500.40       | 9.34  | 405.07  | --      |
| NN     | 0.32      | 20.29     | 1508.47 | 326.81          | 1.69  | 116.66  | 5.60    |
| SM     | 0.22      | 14.54     | 258.17  | 9.36            | 0.97  | 36.28   | 3.59    |
| NSM    | 0.53      | 166.85    | 4697.24 | 132370.07       | 11.36 | 5535.86 | --      |

Table 3: Performances of the four SMD variants in terms of MSE.

| Kernel                               | Synthetic   | Riverflow   | Sunspot       | CO <sub>2</sub> | Ozone       | Air          | Abalone     |
|--------------------------------------|-------------|-------------|---------------|-----------------|-------------|--------------|-------------|
| SMD ( $\theta=0, \phi=0$ )           | 0.25        | 10.76       | 173.52        | 1.19            | <b>0.59</b> | <b>10.02</b> | 3.29        |
| SMD ( $\theta \neq 0, \phi=0$ )      | 0.21        | 10.70       | 170.39        | <b>0.63</b>     | 0.66        | 32.67        | <b>3.24</b> |
| SMD ( $\theta=0, \phi \neq 0$ )      | 0.20        | 8.44        | 189.30        | 2.80            | 0.79        | 21.08        | 3.33        |
| SMD ( $\theta \neq 0, \phi \neq 0$ ) | <b>0.06</b> | <b>7.85</b> | <b>150.04</b> | <b>0.63</b>     | 0.83        | 12.06        | 3.35        |

Table 4: Performances of baselines in terms of NLML.

| Kernel | Synthetic    | Riverflow | Sunspot  | CO <sub>2</sub> | Ozone  | Air       | Abalone  |
|--------|--------------|-----------|----------|-----------------|--------|-----------|----------|
| LIN    | 343.11       | 949.97    | 1005.43  | 451.38          | 235.68 | 462.01    | 24261.35 |
| SE     | 302.26       | 973.49    | 898.44   | 399.90          | 208.53 | 456.68    | 21246.86 |
| Poly   | 343.10       | 1288.94   | 1097.68  | 1444.80         | 375.86 | 735.39    | 17964.17 |
| PER    | 340.25       | 938.97    | 1005.33  | 459.53          | 236.71 | 456.38    | 18775.23 |
| RQ     | 302.26       | 888.33    | 884.69   | 222.17          | 196.96 | 430.86    | 15988.48 |
| MA     | 272.50       | 951.67    | 888.91   | 278.33          | 208.17 | 451.03    | 20288.56 |
| Gabor  | 302.26       | 1031.72   | 1095.35  | 1444.62         | 240.55 | 735.41    | 15400.84 |
| FBM    | <b>66.55</b> | 927.39    | 914.56   | 910.61          | 202.42 | 457.79    | --       |
| ULL    | 146.07       | 888.33    | 934.21   | 819.09          | 206.85 | 441.31    | --       |
| NN     | 124.74       | 941.79    | 1002.43  | 460.73          | 225.46 | 449.31    | 17695.80 |
| SM     | 182.48       | 800.95    | 872.97   | 62.09           | 160.75 | 328.56    | 8607.99  |
| NSM    | 4057.48      | 8900.86   | 58251.07 | 8598445.66      | 628.85 | 193932.91 | --       |

Table 5: Performances of the four SMD variants in terms of NLML.

| Kernel                                  | Synthetic     | Riverflow     | Sunspot       | CO <sub>2</sub> | Ozone         | Air           | Abalone        |
|---|---------------|---------------|---------------|-----------------|---------------|---------------|----------------|
| SMD<br>( $\theta = 0, \phi = 0$ )       | 191.46        | 784.99        | 850.27        | 64.34           | 160.48        | <b>300.69</b> | 8566.35        |
| SMD<br>( $\theta \neq 0, \phi = 0$ )    | <b>176.57</b> | 797.49        | <b>845.32</b> | 67.60           | 159.15        | 304.13        | 8717.45        |
| SMD<br>( $\theta = 0, \phi \neq 0$ )    | 191.61        | 752.31        | 848.67        | <b>54.39</b>    | 161.93        | 312.41        | 8935.25        |
| SMD<br>( $\theta \neq 0, \phi \neq 0$ ) | 185.78        | <b>737.32</b> | 861.02        | 65.55           | <b>154.32</b> | 307.74        | <b>6831.01</b> |

interference. For instance, in the monthly river flow extrapolation task, the moon and sun are primarily responsible for the rising and falling of river tidal flows which are delayed and augmented under the influence of gravity and resonances. Results of experiments on these datasets show the benefits of the SMD variant with  $\theta \neq 0, \phi \neq 0$  to improve performance when modeling natural phenomena with very limited human intervention. This is further demonstrated by results on the other considered datasets (CO<sub>2</sub>, Ozone and Air), which stem from phenomena involving some form of human intervention, where a lower or no difference in performance over the SMD time and phase delay variants can be observed. For instance the rising trend of CO<sub>2</sub> and of ozone is caused by intensive industry emission, hence by human intervention. The time evolution patterns of such human intervention driven phenomena contained in the considered datasets indicate a simpler form of statistical dependency between components. On these datasets the performance of SMD with  $\theta \neq 0$  and  $\phi \neq 0$  is comparable to that of the other SMD variants ( $\theta = 0$  or  $\phi = 0$ , see Table 3).

From Tables 2, 3 and Tables 4, 5 we can see that a lower NLML does not corresponds to better extrapolation results for unseen points. While the MSE results for SMD are better than those of other kernels, the NLML of SMD is not always the lowest one. The reason is that both SM and SMD have more hyper-parameters, thus the marginal likelihood surfaces for the GPs of SM and SMD may have many more local optima. Also, a lower NLML values with larger MSE corresponding to a local optima perhaps may be caused by overfitting, which leads to poor extrapolation performance on unseen points. In general NLML is the sum of two terms (and a constant term that is ignored): a model fit and a complexity penalty term. The first term is the data fit term which is maximized when the data fits the model very well. The second term is a penalty on the complexity of the model, i.e. the smoother the better. When Optimizing NLML finds a balance between the two and this changes with the data observed.

Results show unsatisfactory performance of NSM on the synthetic dataset containing dependent structures, as well as on real-world datasets (note that NSM is not applicable for non-Cartesian multidimensional, i.e.  $P > 2$ , datasets). These results can be justified by the higher number of hyper-parameters of NSM, at least three times the number of hyper-parameters of SM, since in NSM each hyper-parameter of SM is parameterized as a Gaussian function with additional three hyper-parameters. Thus on small datasets, NSM tends to suffer from overfitting. In general, GP models with a high number of hyper-parameters require a large training data in order to perform optimization on high dimensional marginal likelihood surfaces.

## 8 Conclusion

We introduced the SMD kernel, which extends the SM kernel by incorporating time and phase delay dependencies between components. SMD generalizes SM by discarding its implicit assumption that components are *a priori* independent. Using the posterior correlation, introduced in previous work to quantify statistical dependencies in additive kernels, we have shown the presence of statistical dependencies between components in the SM kernel and motivated the proposed kernel extension. We showed empirically that such dependencies are beneficial for modeling predictive trends and for decreasing uncertainty.

The proposed SMD kernel decomposes each SM component in the frequency domain and provides a way to explicitly model correlations between components. The cross spectral density is constructed by a product of basis spectral density and complex conjugate of another basis spectral density in the frequency domain. In SMD dependencies between components are expressed using cross convolution which we used to define the  $\gamma_{ij}$  coefficient for quantifying the dependency between components  $i$  and  $j$  captured by SMD.

Results of extensive experiments on artificial and real-life datasets indicate that SMD is capable to capture time and phase delay dependencies between components through convolution. Results also show that SMD can identify and model involved structure in the data and perform accurate forecasting of long-term trends. The beneficial effects of SMD are shown to be stronger when modeling natural phenomena involving very limited or no human intervention.

There are two main problems which remain to be addressed in future work. A main issue is the initialization of time and phase delay parameters. Here we just used random initialization. However, more tailored, effective methods remain to be investigated. Another issue, common to all GP methods, is the problem of sparse or efficient inference [24, 23, 33, 34], which needs to be improved also for GPs with SMD. Lévy process priors as proposed in [35] present a promising approach for tackling this problem, by regularizing spectral mixture for automatic selection of the number of components and pruning of unnecessary components.

## A Empirical analysis of statistical dependency between SM components

Step by step, we illustrate the presence of dependencies between components using the monthly river flow dataset described in Section 7.2, including the experimental setting. Here we perform extrapolation using an SM kernel with  $Q = 6$  components and consider its decomposition in terms of SM components to illustrate the presence of dependencies between components. Specifically, we 1) train a GP using an SM kernel with  $Q = 6$  components on the monthly river flow dataset; 2) compute  $f_i^*$  for  $i = 1, \dots, Q$ ; 3) compute predictions using (sum of)  $f_i^*$ 's conditioned to sum of  $f_i$ 's: (a)  $f_i^*|f_i$ , (b)  $f_i^*|\sum_{j=1}^Q f_j$ , (c)  $\sum_{i=1}^q (f_i^*|f_i)$ , (d)  $\sum_{i=1}^q f_i^*|\sum_{i=1}^q f_i$ , (e)  $\sum_{i=1}^q (f_i^*|\sum_{j=1}^Q f_j)$  where  $1 \leq q \leq Q$ . In all figures below training, testing, SM, and confidence interval are plotted in black, green, dashed red, and gray, respectively.

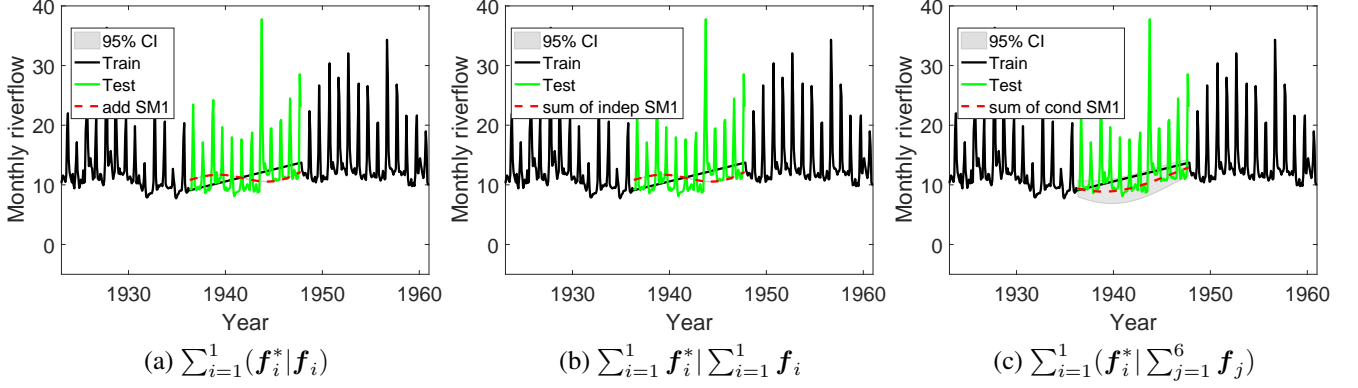


Figure 20: (a) Cumulative sum of the first 1 SM component's extrapolation; (b) The extrapolation of the cumulative sum of 1 SM component; (c) Extrapolation using the sum of the extrapolation of 1 SM component which condition on the sum of all SM components.

The 1st SM component describes the linear rising tendency of riverflow levels. The extrapolation of 1st SM component  $f_1^*|f_1$  and the extrapolation of 1st SM component conditioned on the cumulative sum of all SM components  $f_1^*|\sum_{i=1}^6 f_i$  are shown in Figure 1. In this case,  $f_1^*|\sum_{i=1}^6 f_i$  with bigger confidence interval and corrected trend is not equal to  $f_1^*|f_1$ , while  $\sum_{i=1}^1 (f_i^*|f_i)$  is equal to  $\sum_{i=1}^1 f_i^*|\sum_{i=1}^1 f_i$  and  $f_1^*|\sum_{i=1}^6 f_i$  is equal to  $\sum_{i=1}^1 (f_i^*|\sum_{j=1}^6 f_j)$ .

The 2nd SM component presents a long term pattern with larger fluctuated values at the beginning and end of the predictive interval. However  $f_2^*|\sum_{i=1}^6 f_i$  reduced the larger prediction of  $f_2^*|f_2$  with almost zero values. Here the difference between  $\sum_{i=1}^2 (f_i^*|f_i)$  and  $\sum_{i=1}^2 f_i^*|\sum_{i=1}^2 f_i$  is significant, which means that the posterior covariance in SM kernel corrects the extrapolation and changed the predictive distribution. As a result of very small predictive values in subplot (b)  $f_2^*|\sum_{i=1}^6 f_i$ , subplot (e)  $\sum_{i=1}^2 (f_i^*|\sum_{j=1}^6 f_j)$  still keeps the linear rising trends.

The 3rd SM component characterizes the periodical short-term smoothness of riverflow levels. However  $f_3^*|\sum_{i=1}^6 f_i$  increased the small prediction of  $f_3^*|f_3$ . Here the difference between  $\sum_{i=1}^3 (f_i^*|f_i)$  and  $\sum_{i=1}^3 f_i^*|\sum_{i=1}^3 f_i$  is significant, which means that the posterior covariance in SM kernel corrects the extrapolation and changed the predictive distribution. Incorporating periodical trends  $f_3^*|\sum_{i=1}^6 f_i$  in the linear rising trends, subplot (e)  $\sum_{i=1}^3 (f_i^*|\sum_{j=1}^6 f_j)$  gives a periodical linear raising trends.

The 4th SM component is a quasi-periodical trend with oscillating peaks in the predictive header and predictive trailer. While the extrapolation of the 4th SM component conditioned on the sum of SM components becomes almost a smooth and steady linear trend with much less variation. Therefore compared with Figure 22 subplot (e), trends in  $\sum_{i=1}^4 (f_i^*|\sum_{j=1}^6 f_j)$  do not change very much. Particularly  $f_4^*|f_4$  makes larger contribution to  $\sum_{i=1}^4 (f_i^*|f_i)$ , while  $f_4^*|\sum_{i=1}^6 f_i$  makes very small contribution. The difference between  $f_4^*|f_4$  and  $f_4^*|\sum_{i=1}^6 f_i$  and the difference between  $\sum_{i=1}^4 (f_i^*|f_i)$  and  $\sum_{i=1}^4 f_i^*|\sum_{i=1}^4 f_i$  are significant.

The 5th SM component captures a similar patterns with the 2nd SM component, but has smaller amplitude of oscillating peaks (see subplot (2), Figure 24). Similarly, when the 5th SM component conditioned on the sum of all SM components, the extrapolation was nearly corrected and reduced as a smooth and linear trend with a downtrend at the beginning of the predictive interval and an uptrend at the end of the predictive interval. Here the extrapolations of  $\sum_{i=1}^5 (f_i^*|f_i)$ ,

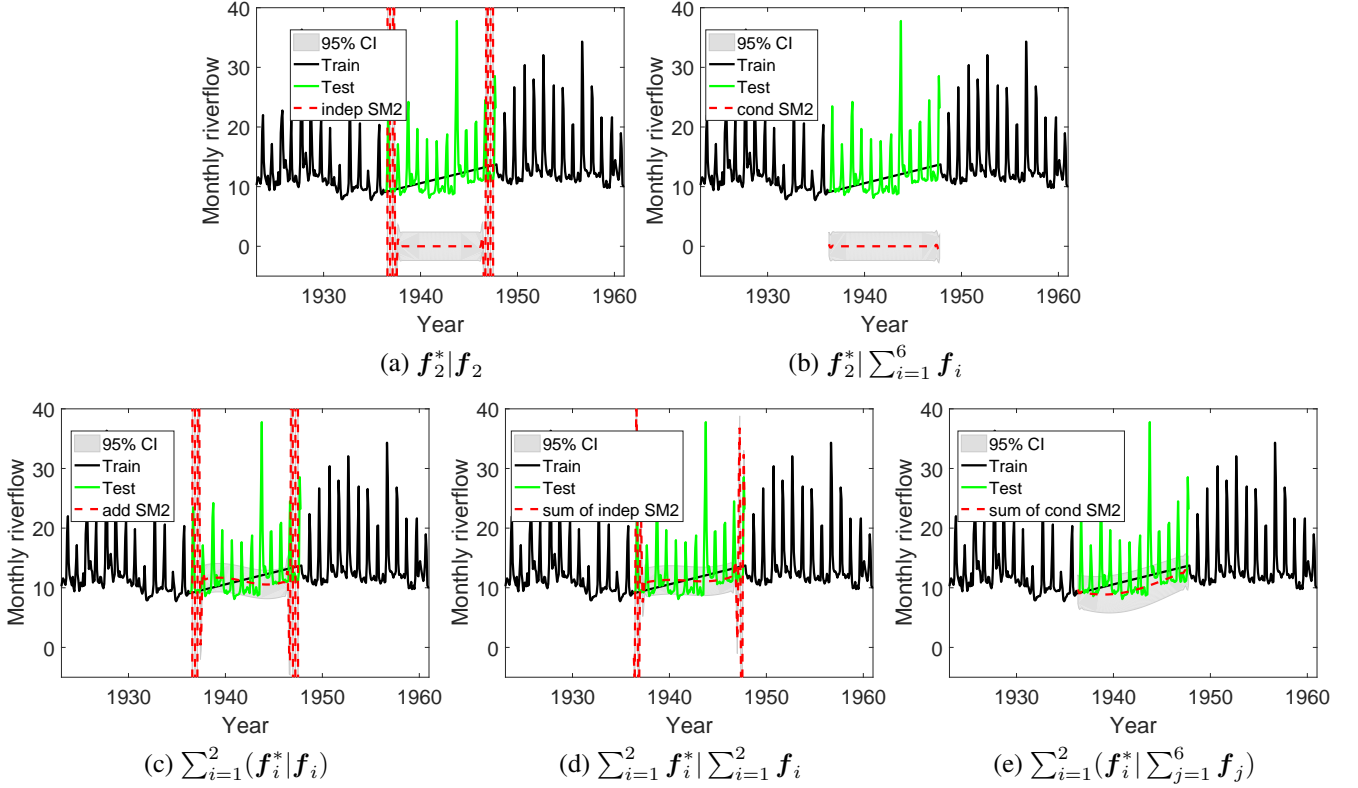


Figure 21: (a) The extrapolation of 2nd SM component; (b) The extrapolation of 2nd SM component conditioned on the cumulative sum of all SM components; (c) Cumulative sum of the first 2 SM components extrapolation; (d) The extrapolation of the cumulative sum of 2 SM components; (e) Extrapolation using the sum of the extrapolation of 2 SM components which condition on the sum of all SM components.

$\sum_{i=1}^5 \mathbf{f}_i^* | \sum_{i=1}^5 \mathbf{f}_i$ , and  $\sum_{i=1}^5 (\mathbf{f}_i^* | \sum_{j=1}^6 \mathbf{f}_j)$  are changed much because of the significant contribution of 5th SM components.

The 6th SM component learned a quasi-periodical trend with relative stable period and unstable big amplitude. Similarly, when the 6th SM component conditioned on the sum of all SM components, the extrapolation was nearly corrected as a periodical trend with stable amplitude. The contributions of  $\mathbf{f}_6^* | \mathbf{f}_6$  to  $\sum_{i=1}^6 (\mathbf{f}_i^* | \mathbf{f}_i)$ ,  $\mathbf{f}_6^* | \sum_{i=1}^6 \mathbf{f}_i$  to  $\sum_{i=1}^6 \mathbf{f}_i^* | \sum_{i=1}^6 \mathbf{f}_i$ , and  $\mathbf{f}_6^* | \sum_{i=1}^6 \mathbf{f}_i$  to  $\sum_{i=1}^6 (\mathbf{f}_i^* | \sum_{j=1}^6 \mathbf{f}_j)$  are significant. Note that  $\sum_{i=1}^6 \mathbf{f}_i^* | \sum_{i=1}^6 \mathbf{f}_i$  and  $\sum_{i=1}^6 (\mathbf{f}_i^* | \sum_{j=1}^6 \mathbf{f}_j)$  in fact are the same, which is the final predictive distribution (see Figure 6) of whole SM kernel which in practical makes use of and benefits from the posterior covariance (see Equation (12)).

In summary, these interesting characteristics of dependency in SM kernel show that the posterior covariance between components not only exist but also contributes substantially on trends learning as well as increasing uncertainty.

## References

- [1] Carl Edward Rasmussen and Hannes Nickisch. Gaussian processes for machine learning (gpml) toolbox. *Journal of Machine Learning Research*, 11(Nov):3011–3015, 2010.
- [2] Carl Edward Rasmussen and Christopher KI Williams. *Gaussian process for machine learning*. MIT press, 2006.
- [3] Andrew Wilson and Ryan Adams. Gaussian process kernels for pattern discovery and extrapolation. In *Proceedings of the 30th International Conference on Machine Learning (ICML-13)*, pages 1067–1075, 2013.
- [4] Sami Remes, Markus Heinonen, and Samuel Kaski. Non-stationary spectral kernels. In *Advances in Neural Information Processing Systems*, pages 4645–4654, 2017.

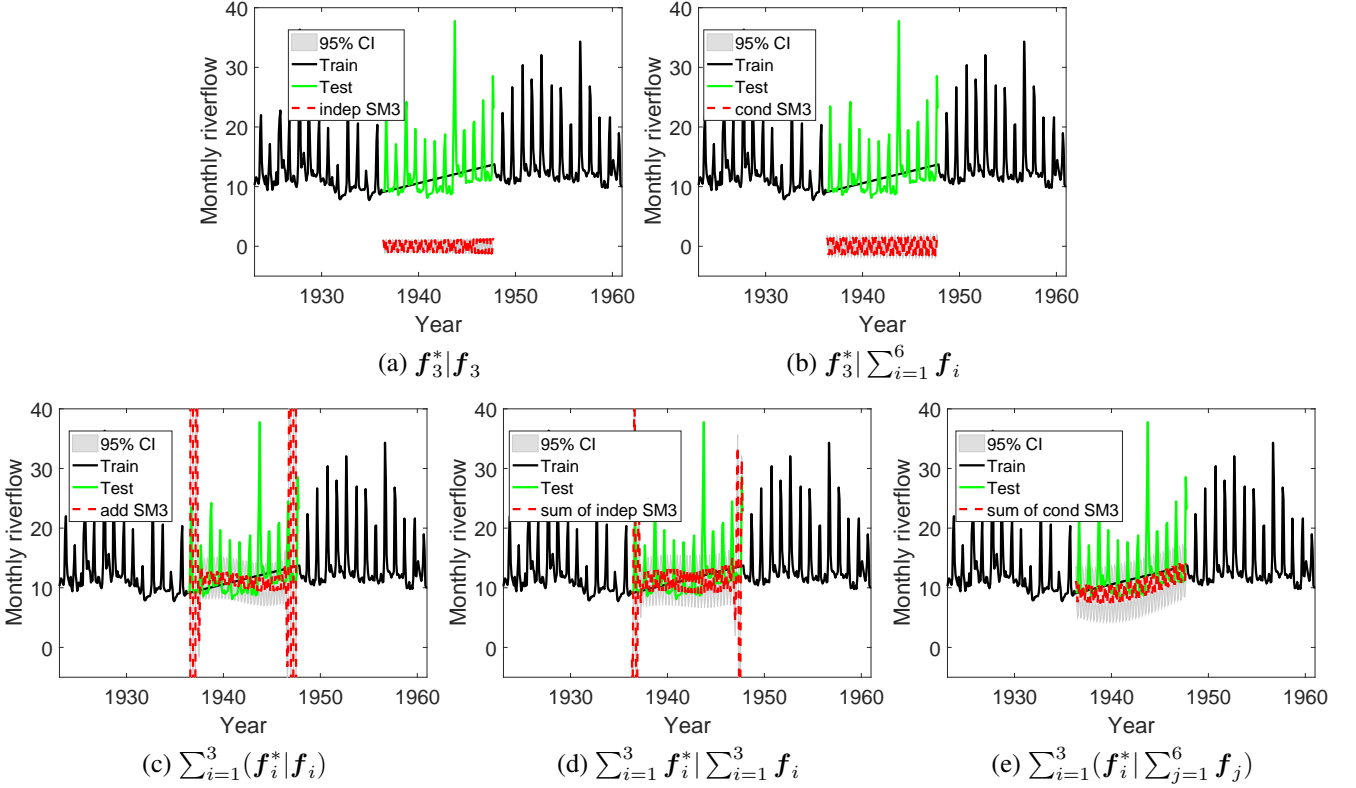


Figure 22: (a) The extrapolation of 3rd SM component; (b) The extrapolation of 3rd SM component conditioned on the cumulative sum of all SM components; (c) Cumulative sum of the first 3 SM components extrapolation; (d) The extrapolation of the cumulative sum of 3 SM components; (e) Extrapolation using the sum of the extrapolation of 3 SM components which condition on the sum of all SM components.

[5] Andrew G Wilson, Elad Gilboa, Arye Nehorai, and John P Cunningham. Fast kernel learning for multidimensional pattern extrapolation. In *Advances in Neural Information Processing Systems*, pages 3626–3634, 2014.

[6] Li-Fang Cheng, Gregory Darnell, Corey Chivers, Michael E Draugelis, Kai Li, and Barbara E Engelhardt. Sparse multi-output Gaussian processes for medical time series prediction. *arXiv preprint arXiv:1703.09112*, 2017.

[7] Matthew Kupilik, Frank Witmer, Euan-Angus MacLeod, Caixia Wang, and Tom Ravens. Gaussian process regression for arctic coastal erosion forecasting. *arXiv preprint arXiv:1712.00867*, 2017.

[8] Xiuming Liu, Teng Xi, and Edith Ngai. Data modelling with Gaussian process in sensor networks for urban environmental monitoring. In *Modeling, Analysis and Simulation of Computer and Telecommunication Systems (MASCOTS), 2016 IEEE 24th International Symposium on*, pages 457–462. IEEE, 2016.

[9] David Duvenaud. *Automatic model construction with Gaussian processes*. PhD thesis, University of Cambridge, 2014.

[10] Salomon Bochner. *Lectures on Fourier Integrals.(AM-42)*, volume 42. Princeton University Press, 2016.

[11] ML Stein. Interpolation of spatial data: some theory for kriging., 1999.

[12] David Duvenaud, James Robert Lloyd, Roger Grosse, Joshua B Tenenbaum, and Zoubin Ghahramani. Structure discovery in nonparametric regression through compositional kernel search. *arXiv preprint arXiv:1302.4922*, 2013.

[13] William Herlands, Andrew Wilson, Hannes Nickisch, Seth Flaxman, Daniel Neill, Wilbert Van Panhuis, and Eric Xing. Scalable Gaussian processes for characterizing multidimensional change surfaces. In *Artificial Intelligence and Statistics*, pages 1013–1021, 2016.

[14] Jasper Snoek, Hugo Larochelle, and Ryan P Adams. Practical Bayesian optimization of machine learning algorithms. In *Advances in neural information processing systems*, pages 2951–2959, 2012.

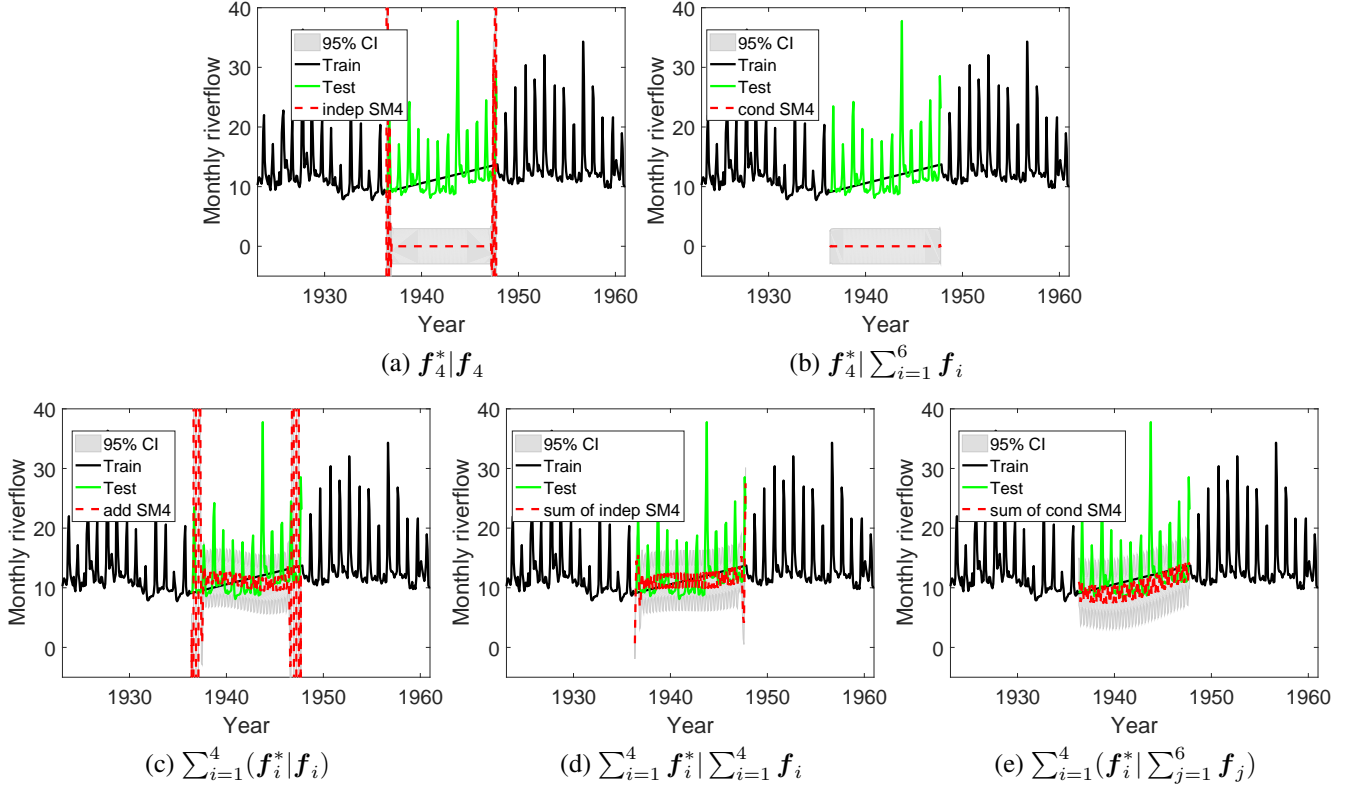


Figure 23: (a) The extrapolation of 4th SM component; (b) The extrapolation of 4th SM component conditioned on the cumulative sum of all SM components; (c) Cumulative sum of the first 4 SM components extrapolation; (d) The extrapolation of the cumulative sum of 4 SM components; (e) Extrapolation using the sum of the extrapolation of 4 SM components which condition on the sum of all SM components.

[15] Kai Chen, Twan van Laarhoven, Jinsong Chen, and Elena Marchiori. Incorporating dependencies in spectral kernels for Gaussian processes. In *Machine Learning and Knowledge Discovery in Databases - European Conference, ECML PKDD 2019, Wrzburg, Germany, 2019, Proceedings*, 2019.

[16] Gabriel Parra and Felipe Tobar. Spectral mixture kernels for multi-output Gaussian processes. In Isabelle Guyon, Ulrike von Luxburg, Samy Bengio, Hanna M. Wallach, Rob Fergus, S. V. N. Vishwanathan, and Roman Garnett, editors, *Advances in Neural Information Processing Systems 30: Annual Conference on Neural Information Processing Systems 2017, 4-9 December 2017, Long Beach, CA, USA*, pages 6684–6693, 2017.

[17] Harry Bateman. *Tables of integral transforms [volumes I & II]*, volume 1. McGraw-Hill Book Company, 1954.

[18] Gregory Gaspari and Stephen E Cohn. Construction of correlation functions in two and three dimensions. *Quarterly Journal of the Royal Meteorological Society*, 125(554):723–757, 1999.

[19] Anandamayee Majumdar and Alan E Gelfand. Multivariate spatial modeling for geostatistical data using convolved covariance functions. *Mathematical Geology*, 39(2):225–245, 2007.

[20] Marc G Genton, William Kleiber, et al. Cross-covariance functions for multivariate geostatistics. *Statistical Science*, 30(2):147–163, 2015.

[21] MI Yadrenko. *Correlation theory of stationary and related random functions, vol i, basic results*, 1987.

[22] Harald Cramér. On the theory of stationary random processes. *Annals of Mathematics*, pages 215–230, 1940.

[23] Edward Snelson and Zoubin Ghahramani. Sparse Gaussian processes using pseudo-inputs. In *Advances in neural information processing systems*, pages 1257–1264, 2006.

[24] Joaquin Quiñero-Candela and Carl Edward Rasmussen. A unifying view of sparse approximate Gaussian process regression. *Journal of Machine Learning Research*, 6(Dec):1939–1959, 2005.

[25] Christopher KI Williams and Matthias Seeger. Using the nyström method to speed up kernel machines. In *Advances in neural information processing systems*, pages 682–688, 2001.

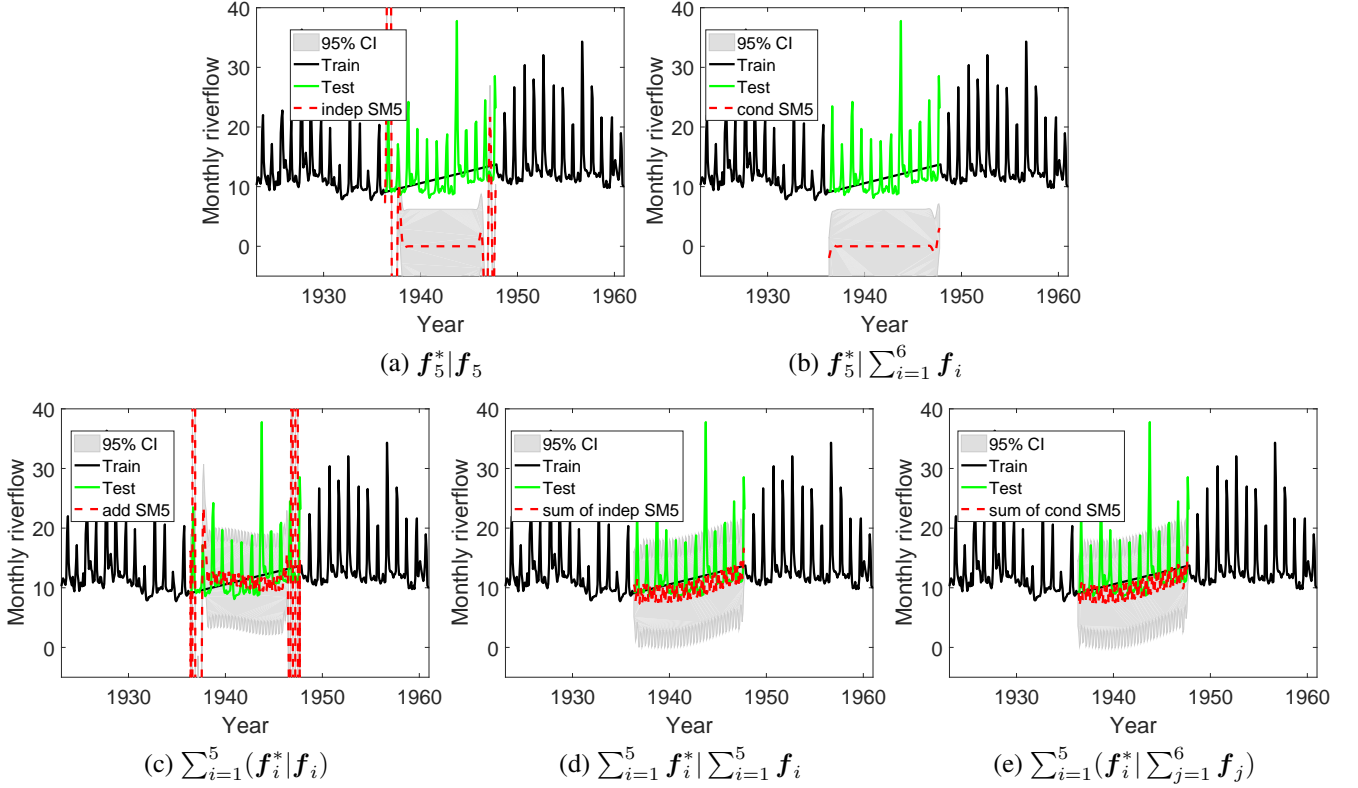


Figure 24: (a) The extrapolation of 5th SM component; (b) The extrapolation of 5th SM component conditioned on the cumulative sum of all SM components; (c) Cumulative sum of the first 5 SM components extrapolation; (d) The extrapolation of the cumulative sum of 5 SM components; (e) Extrapolation using the sum of the extrapolation of 5 SM components which condition on the sum of all SM components.

[26] James Hensman, Nicol  Fusi, and Neil D. Lawrence. Gaussian processes for big data. In Ann Nicholson and Padhraic Smyth, editors, *Proceedings of the Twenty-Ninth Conference on Uncertainty in Artificial Intelligence, UAI 2013, Bellevue, WA, USA, August 11-15, 2013*. AUAI Press, 2013.

[27] James Hensman, Nicolas Durrande, and Arno Solin. Variational fourier features for Gaussian processes. *Journal of Machine Learning Research*, 18:151:1–151:52, 2017.

[28] Toad K Moon. The expectation-maximization algorithm. *IEEE Signal Processing Magazine*, 13(6):47–60, 1997.

[29] Charles D Keeling. Atmospheric co<sub>2</sub> records from sites in the sio air sampling network. *Trends’ 93: A compendium of data on global change*, pages 16–26, 1994.

[30] Alexander G de G Matthews, Mark van der Wilk, Tom Nickson, Keisuke Fujii, Alexis Boukouvalas, Pablo Le n-Villagr , Zoubin Ghahramani, and James Hensman. GPflow: A Gaussian process library using tensorflow. *Journal of Machine Learning Research*, 18(40):1–6, 2017.

[31] Keith W Hipel and A Ian McLeod. *Time series modelling of water resources and environmental systems*, volume 45. Elsevier, 1994.

[32] R. C. Willson, S. Gulkis, M. Janssen, H. S. Hudson, and G. A. Chapman. Observations of solar irradiance variability. *Science*, 211(4483):700–702, 1981.

[33] Andrew Gordon Wilson and Hannes Nickisch. Kernel interpolation for scalable structured Gaussian processes (KISS-GP). In Francis R. Bach and David M. Blei, editors, *Proceedings of the 32nd International Conference on Machine Learning, ICML 2015, Lille, France, 6-11 July 2015*, volume 37 of *JMLR Workshop and Conference Proceedings*, pages 1775–1784. JMLR.org, 2015.

[34] Jacob R Gardner, Geoff Pleiss, Ruihan Wu, Kilian Q Weinberger, and Andrew Gordon Wilson. Product kernel interpolation for scalable Gaussian processes. *arXiv preprint arXiv:1802.08903*, 2018.

[35] Phillip A Jang, Andrew Loeb, Matthew Davidow, and Andrew G Wilson. Scalable Levy process priors for spectral kernel learning. In *Advances in Neural Information Processing Systems*, pages 3943–3952, 2017.

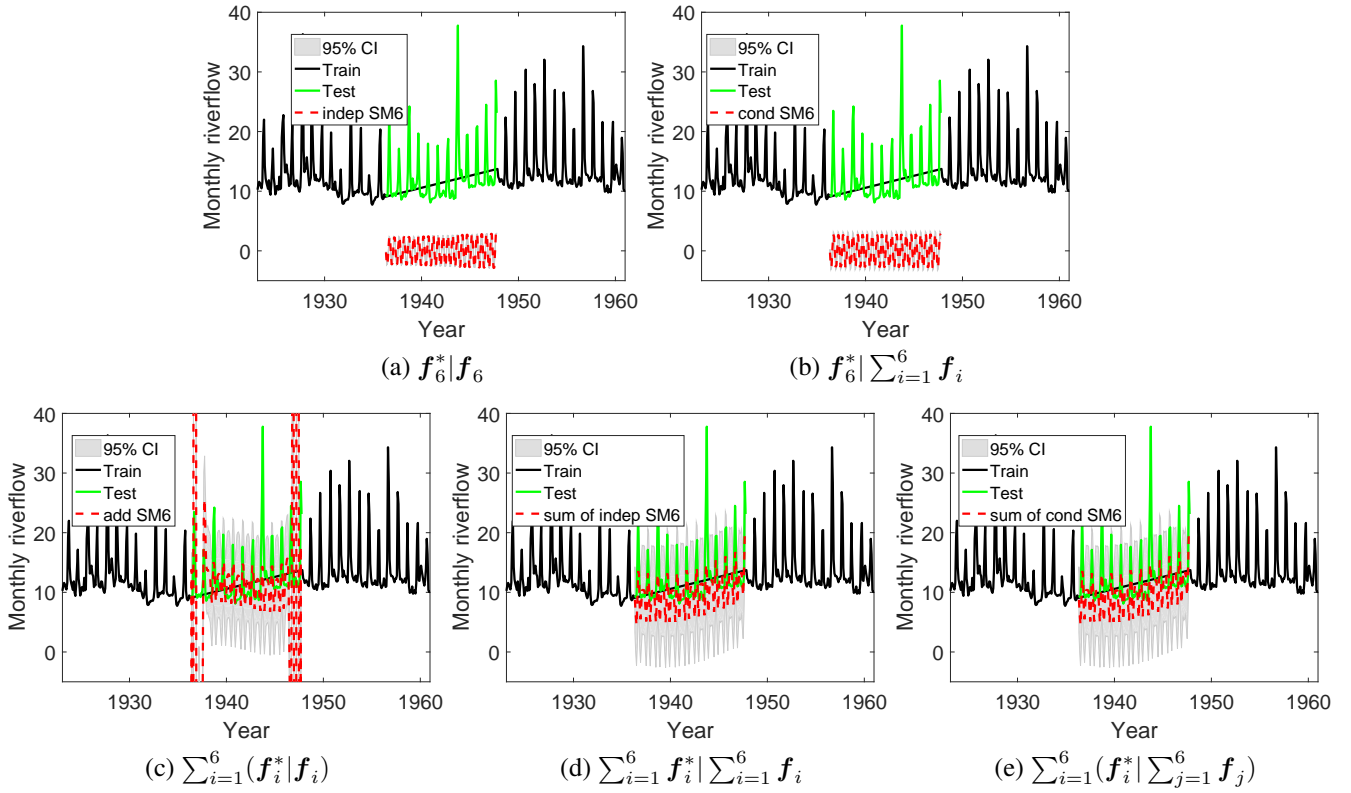


Figure 25: (a) The extrapolation of 6th SM component; (b) The extrapolation of 6th SM component conditioned on the cumulative sum of all SM components; (c) Cumulative sum of the first 6 SM components extrapolation; (d) The extrapolation of the cumulative sum of 6 SM components; (e) Extrapolation using the sum of the extrapolation of 6 SM components which condition on the sum of all SM components.